Bioactive Materials 34 (2024) 422–435

Contents lists available at ScienceDirect

Bioactive Materials

journal homepage: www.keaipublishing.com/en/journals/bioactive-materials

Targeted chemotherapy via HER2-based chimeric antigen receptor (CAR) engineered T-cell membrane coated polymeric nanoparticles

Serkan Yaman [a,c,1], Harish Ramachandramoorthy [a,c,1], Priyanka Iyer [a], Uday Chintapula [a,c], Tam Nguyen [a], Manoj Sabnani [b], Tanviben Kotadia [b], Soroush Ghaffari [e], Laurentiu M. Pop [d], Raquibul Hannan [d], Jon A. Weidanz [a,e,**], Kytai T. Nguyen [a,*]

[a] Department of Bioengineering, University of Texas at Arlington, TX, USA
[b] Department of Biology, University of Texas at Arlington, TX, USA
[c] Joint Bioengineering Program, University of Texas Southwestern Medical Center, TX, USA
[d] Department of Radiation Oncology, University of Texas Southwestern Medical Center, TX, USA
[e] Department of Kinesiology, University of Texas at Arlington, Arlington, TX, USA

ARTICLE INFO

Keywords:
Nanoparticles
CAR-T cells
Membrane-based drug delivery
Cancer chemotherapy

ABSTRACT

Cell membrane-derived nanoparticles (NPs) have recently gained popularity due to their desirable features in drug delivery such as mimicking properties of native cells, impeding systemic clearance, and altering foreign body responses. Besides NP technology, adoptive immunotherapy has emerged due to its promise in cancer specificity and therapeutic efficacy. In this research, we developed a biomimetic drug carrier based on chimeric antigen receptor (CAR) transduced T-cell membranes. For that purpose, anti-HER2 CAR-T cells were engineered via lentiviral transduction of anti-HER2 CAR coding lentiviral plasmids. Anti-HER2 CAR-T cells were characterized by their specific activities against the HER2 antigen and used for cell membrane extraction. Anti-cancer drug Cisplatin-loaded poly (D, L-lactide-*co*-glycolic acid) (PLGA) NPs were coated with anti-human epidermal growth factor receptor 2 (HER2)-specific CAR engineered T-cell membranes. Anti-HER2 CAR-T-cell membrane-coated PLGA NPs (CAR-T-MNPs) were characterized and confirmed via fluorescent microscopy and flow cytometry. Membrane-coated NPs showed a sustained drug release over the course of 21 days in physiological conditions. Cisplatin-loaded CAR-T-MNPs also inhibited the growth of multiple HER2+ cancer cells *in vitro*. In addition, *in vitro* uptake studies revealed that CAR-T-MNPs showed an increased uptake by A549 cells. These results were also confirmed via *in vivo* biodistribution and therapeutic studies using a subcutaneous lung cancer model in nude mice. CAR-T-MNPs localized preferentially at tumor areas compared to those of other studied groups and consisted of a significant reduction in tumor growth in tumor-bearing mice. In Conclusion, the new CAR modified cell membrane-coated NP drug-delivery platform has demonstrated its efficacy both *in vitro* and *in vivo*. Therefore, CAR engineered membrane-coated NP system could be a promising cell-mimicking drug carrier that could improve therapeutic outcomes of lung cancer treatments.

1. Introduction

Lung cancer, the deadliest form of cancer accounting for nearly 1.6 million cases around the world annually, has a less than 15% five-year survival rate [1–3]. Conventional treatment strategies such as surgery, radiation therapy (RT), and chemotherapy (CT) have limitations, including frequent relapse and severe side effects such as hair loss, nausea, fatigue, and nerve damage [4,5]. Surgical removal of tumors is not always feasible in some patients with lung cancer [6]; for example, 30–40% of non-small-cell lung cancer (NSCLC) patients have unresectable tumors [7,8]. For many years, the main treatments have been RT and CT, and despite many technological advances, the five-year overall

Peer review under responsibility of KeAi Communications Co., Ltd.
* Corresponding author. Department of Bioengineering, University of Texas at Arlington, 500 UTA Blvd, ERB 241, Arlington, TX, 76019, USA.
** Corresponding author. Department of Kinesiology, University of Texas at Arlington, 655W Mitchell St, Arlington, TX, 76019, USA.
E-mail addresses: weidanz@uta.edu (J.A. Weidanz), knguyen@uta.edu (K.T. Nguyen).
[1] Authors contributed equally.

https://doi.org/10.1016/j.bioactmat.2023.12.027
Received 4 August 2023; Received in revised form 29 December 2023; Accepted 29 December 2023

survival rate for these patients still remains low [9,10]. In addition to low survival rates, patients suffer from serious adverse effects during treatment. For instance, CT drugs cause systemic toxicity during their circulation/treatment process. To precisely reach lung tumors while avoiding systemic organ toxicity, a more robust and cell-specific drug delivery system needs to be designed. Novel drug delivery systems such as nanoparticle (NP)-based drug delivery can provide better drug accumulation at a tumor site and take on a cancer cell-specific approach rather than a systemic one [11–13]. These strategies can be used for delivering CT drugs to lung cancer cells for effective, localized treatment.

NP-based drug delivery has not yet fully been controlled and applied clinically for many reasons such as opsonization from a mononuclear phagocytosis system, non-specific clearance [14], relatively short circulation time [15], and limitations of fabricating actively targeted drug carriers. Moreover, the interactions of these synthetic NPs with blood components are another factor that affects the NPs' outcome. This interaction creates a layer on the synthetic surface of NPs called "protein corona" (PC) [16]. PC is responsible for cellular uptake, physiological features, immune responses, and targeting efficiency of NPs [17–19]. For these reasons, using very well-characterized carrier materials and identifying the blood component interactions, as well as their PC composition, is needed for targeted drug delivery applications [20–26]. The above-mentioned shortcomings in the synthetic particle-based drug delivery field make the use of biomimetic materials necessary in creating advanced drug delivery systems [27–30].

Bacteria or virus-based carriers [26,31], hybrid nano-bio systems [32,33], and cell-based drug delivery vehicles [34–36] have been reported to have potential applications for biomimetic-targeted drug delivery. The concept of using cell membranes as drug delivery vehicles is becoming more popular [37–39]. As mentioned earlier, cell membrane-coated drug carriers might ensure unique drug delivery features and functions via coating of NPs with membranes isolated from different cell types, such as red blood cells, platelets, lymphocytes, and bacteria. Among these cell types, lymphocyte cell membranes have major advantages with respect to cancer treatment. They improve drug delivery efficacy, provide better targeting of cancer cells via camouflaging, and consist of minimal unwanted interactions with complement, reticuloendothelial, and renal system components. Lymphocytes express different types of proteins on their membrane surface to detect diseased or inflamed tissues [40,41]. Furthermore, human lymphocytes express high levels of adhesion molecules to reach affected or activated tissues [42,43], and are more effective in targeting tumor sites [44,45]. Thus, the coating of lymphocyte membranes on the surface of a drug carrier would increase the specific tumor accumulation and facilitate targeted tissue interactions through native lymphocyte cell membrane adhesion and complementary molecules [46,47].

Current applications of membrane-coated carriers include neutrophil membrane-coated NPs for targeting metastatic tumor cells, which express ligands for the cell surface adhesive proteins on neutrophil membranes [48]. In another lymphocyte-specific application, cytotoxic T lymphocyte-coated NPs were used for targeting and treating gastric cancer [49]. Our group has previously shown that a T-cell hybridoma membrane expressing a melanoma-specific anti-gp100/HLA-A2 T-cell receptor showed more than a two-fold increase in tumor retention compared to non-modified NPs when coated onto Trametinib-loaded PLGA NPs [46]. T-lymphocyte membrane-encapsulated poly (D, L-lactide-*co*-glycolic acid) (PLGA) NPs were able to avoid being segregated by lysosomes and retained their lymphocyte coating on the NPs while trapped in endolysosomal compartments [50]. Furthermore, tumor-associated carcinoembryonic antigen chimeric antigen receptor (CAR)-engineered Jurkat T-cells were actively accumulated *in vivo* in liver tumors compared to non-engineered Jurkat T-cells in cell-based therapeutic delivery [51,52]. Therefore, the strategy of targeting molecule (CAR, T-cell receptor (TCR) and single-chain variable fragment (scFv)) engineered lymphocyte cell membrane-coated drug delivery is a promising approach for the biomimetic drug delivery field. This type of cell-based biomimetic drug delivery application might provide a new pathway for individualized medicine applications by applying the patients' own cells for their treatments [34,50,53–56].

In this study, we hypothesize that cancer-specific CAR engineered T-cell membrane-coated NPs (CAR-T-MNPs) for targeted chemotherapeutic treatment of NSCLC could facilitate prolonged circulation and specific accumulation at the tumor site, while avoiding systemic clearance. The overall design is presented in Fig. 1. Here we describe a unique approach combining Cisplatin-loaded PLGA NPs coated with CAR-T-cell membranes from genetically engineered human Jurkat T-cells to target HER2+ lung cancer. There is potential for an increased ability of anti-HER2 CAR-T-MNPs to localize and accumulate at tumor sites that would be otherwise challenging to achieve through current modification and bioconjugation techniques of targeting moieties on NPs. PLGA NPs were chosen due to their sustained drug release profile, biocompatibility, biodegradability, proven efficacy, and both the U.S. Food and Drug Administration (FDA) and European Medical Agency approval to be used as chemotherapeutic drug carrier systems and wide variable drug loading capacities. Cisplatin is an FDA-approved CT drug used in the study, which is effective against lung, ovarian, and breast cancer. Novel CAR-T-MNPs are produced by camouflaging PLGA NPs with anti-HER2 scFv-expressing cellular membranes isolated from genetically modified Jurkat T-cells. Properties of CAR-T-MNPs, including *in vitro* cellular uptake in lung cancer cells and therapeutic killing efficacy as well as *in vivo* biodistribution, targeting and therapeutic efficacies were evaluated using cell culture and animal models in comparison with non-transduced Jurkat T-cell membrane-coated PLGA NPs and blank PLGA NPs.

2. Materials and methods

2.1. Materials

Poly (lactic-co-glycolic acid) (PLGA), (LG 50:50, (M_n 25,000–35,000 Da)), was purchased from Akina Inc (West Lafayette, IN). Polyvinyl alcohol (PVA, MW 15,000–25,000), NHS, bovine serum albumin (BSA), Dulbecco's Modified Eagle's Medium (DMEM), Iscove's Modified Dulbecco's Medium (IMDM), dimethyl formamide (DMF), paraformaldehyde, Protease inhibitor cocktail,1-ethyl-3-(3-dimethylaminopropyl)-carbodiimide (EDC) and Triton R X-100 were obtained from Sigma-Aldrich (St. Louis, MO), and dichloromethane from Merck (Kenilworth, NJ). Cisplatin was received from Cayman Chemicals (Ann Arbor, MI). SDS-PAGE gel, and Mini PVDF transfer packs were bought from Bio-Rad (Hercules, CA). The Mini Extruder Kit was acquired from Avanti Polar Lipids (Alabaster, AL). Formvar-coated copper TEM grids were obtained from Electron Microscopy Sciences (Hatfield, PA). Fetal bovine serum (FBS), 1X trypsin-EDTA, and penicillin-streptomycin were ordered from Invitrogen (Waltham, MA). Other chemicals, if not specified, were obtained from Sigma-Aldrich (St. Louis, MO). All reagents were of analytical grade.

2.2. Cell lines and culture conditions

Lentiviral packaging cell line Lenti-X 293 T was purchased from Takara-Clontech. Alveolar Type 1 (AT1) cells, HEK 293 T-cells, HER2 positive tumor cell lines SKOV-3, and Jurkat E6-1 were received through American Type Culture Collection (ATCC, Manassas, VA). A549 WT, A549 HER2 KO cells were ordered from UBIGENE (Austin, Texas). HEK 283 T, A549 WT, A549 HER2 KO, and SKOV-3 cell lines were cultured in DMEM medium supplemented with 10% heat inactivated (HI) FBS, 100 U/mL penicillin, and 100 μg/mL streptomycin (Invitrogen, Waltham, MA). AT1 cells were cultured in IMDM medium supplemented with 10% HI FBS, 100 U/ml penicillin. Jurkat cells were cultured in GT-T551 medium (Takara Bio, San Jose, CA), supplemented with 10% HI FBS at 37 °C and 5% CO2.

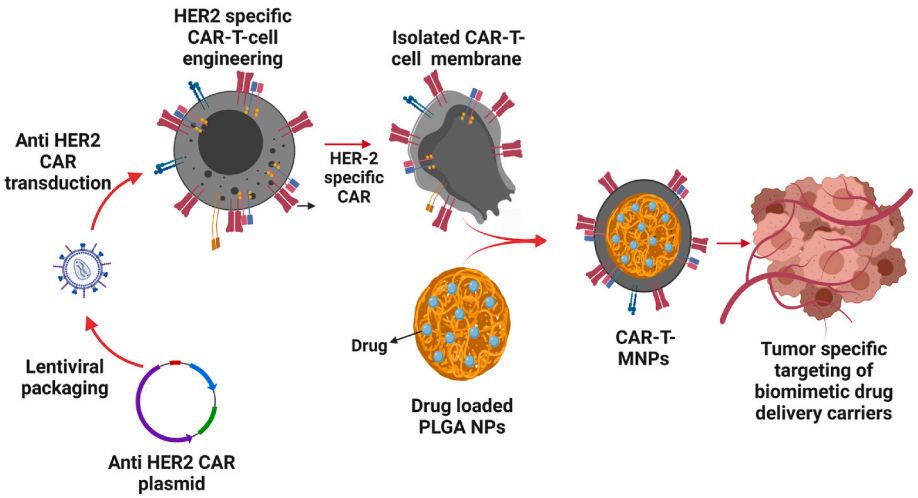

Fig. 1. Overview of proposed CAR-T-MNPs for targeted lung cancer therapy.

2.3. Generation of CAR-T cells

Plasmids including packaging psPAX (Addgene_plasmid #12260) + pLP/VSVG (Invitrogen) and expression plasmids 4GALUAS_tBFP_mCherry (Addgene plasmid #79130) + anti-HER2SynNotch (Addgene plasmid #85424) were used for generating CAR-targeting HER2^{+} (or anti-HER2) cancer cells. The Lenti-X 293T lentiviral packaging cell line was used to generate lentiviral particles, which were employed in our experiments for transduction purposes [57]. Plasmids were transfected into Lenti-X 293T cells via Lipofectamine™ 3000 (Thermofisher). We then optimized the lentiviral particles produced by transfected Lenti-X 293T cells using a viral titer kit (Cell Biolabs Inc.), and multiplicity of infection (MOI) of 1:10 (T-cell: viral particles) was calculated to match the viral titer requirement for Jurkat T-cells which underwent transduction [58,59]. Internal mCherry expression was used for transduction optimization, efficacy, and follow-up studies.

2.4. Synthesis of PLGA nanoparticles

Cisplatin-loaded PLGA nanoparticles (MNPs) were synthesized using a modified version of a standard emulsion protocol [11–13]. Briefly, 10 mg of Cisplatin dissolved in 1 ml of DMF was added dropwise to 3 mL of DMF containing 100 mg of PLGA and sonicated for 2 min. Resultant emulsification was added dropwise to 20 mL of aqueous phase containing 5% poly (vinyl alcohol) and emulsified using ultrasonication for 5 min. The mixture was subsequently stirred and centrifuged at 20,000 RPM for 20 min. The NPs were washed, collected, and freeze-dried. For *in vitro* and *in vivo* uptake and biodistribution studies, 5 μg of Coumarin-6 green dye or Indocyanine green (ICG) infrared dye was added to the PLGA DMF solution instead of Cisplatin during PLGA NP synthesis.

2.5. CAR-T-cell generation and membrane isolation

CAR-T-cells expressing anti-HER2 scFv were created by transduction using lentiviral particles. The CAR-T Jurkat cells (10 [8]) were washed three times with cold PBS (1X). The cells were then counted and resuspended in cold hypotonic buffer Tris-HCl (10 mM, pH7.5) in 10 mL. Protease and phosphatase inhibitor cocktail (PIC) (Sigma Aldrich, St. Louis, MO) was added (5 μL/million cells) and incubated at 4 °C for 20 min. The mixture was centrifuged at 6000 g for 10 min. The resulting pellet was resuspended in cold PBS (0.25X) + PIC at 1 mL/10 million cells and incubated for another 20 min at 4 °C. The mixture was centrifuged at 6000 g for 10 min, then the pellet was resuspended in cold PBS (1X) + PIC and kept on ice. Deoxyribonuclease (DNAse) reaction was performed on the samples based on their DNA contents (20 IU DNAse for 20 million cells for 4 h). The solution was then centrifuged at 6000 g for 10 min. The isolated membranes were collected, lyophilized overnight and stored at 4 °C [46].

2.6. Synthesis of CAR-T-MNPs

CAR-T membrane-derived NPs were prepared as follows: Cisplatin-loaded PLGA NPs were hydrated along with freeze-dried CAR-T membranes, whereas the CAR-T membrane amount was slightly more than the measured amount of lipid molecule derived from cells to cover the entirety of PLGA NP surface. The mixture was sonicated for 5 min using a probe sonicator (Qsonica, Newtown, CT). Subsequently, the mixture was co-extruded using an Avanti mini extruder (Avanti polar lipids, Alabaster, AL), as previously reported [34].

2.7. Physicochemical characterization of CAR-T-MNPs

Dynamic Light Scattering (DLS) technique was used to measure physiochemical characterizations including size, zeta potential, and polydispersity index. To measure the size of the NPs, a suspension of NPs (10 μL of 500 μg/mL) was added to 3 mL of deionized water and measured by the DLS (Brookhaven Instruments, Holtsville, NY) in disposable square cuvette cells. Surface morphology of the formulated NPs was visualized by transmission electron microscopy (TEM). Briefly, freeze-dried NP samples in DI water were fixed onto ozone-treated copper grids (Electron Microscopy Sciences, Hatfield, PA) and stained with uranyl acetate (0.5%) (Sigma Aldrich, St. Louis, MO). A H-7500 TEM (Hitachi, Tokyo, Japan) transmission electron microscope was used to visualize the particle's morphology.

2.8. Characterization of CAR-T membrane coating

After extrusion, to measure the coating efficiency, Coumarin-6-loaded CAR-T-MNPs were stained with lipophilic DiD dye (Thermo Fisher Scientific, Waltham, MA) and analyzed by flow cytometry (red channel). To identify the specific anti-HER2 CAR receptor in the CAR-T-MNP formulations, the particles were stained with Allophycocyanin (APC)-labeled anti c-myc tag antibody (Biolegend, San Diego, CA) to detect scFv on the particle surface.

Western Blot analysis was done to confirm the successful transduction of anti-HER2 CAR molecules on isolated membranes. In Western Blot analysis, isolated membranes were run on SDS-PAGE gels under denaturing conditions. First, membrane proteins were isolated from obtained membrane fractions using Mem-PER plus membrane protein

extraction kit (Thermo Fisher Scientific, Waltham, MA). Samples were mixed with laemmeli buffer containing 10% β-mercaptoethanol, 4% SDS, 125 mM Tris-HCl, 20% glycerol, 0.004% bromophenol blue (Sigma-Aldrich) and run-on gel. Then they were transferred onto nitrocellulose membranes. Then membranes were incubated with the primary antibody against mouse c-myc tag (Biolegend, San Diego, CA) to identify anti-HER2 CAR. Mouse anti-human CD3 zeta antibody (Biolegend, San Diego, CA) was used to detect CD3 zeta membrane protein as a housekeeping protein. Later, membranes were incubated with horseradish peroxidase (HRP)-conjugated secondary anti-mouse IgG antibody (Jackson ImmunoResearch. West Grove, PA). After the washing steps, blots were visualized using the Immobilon ECL (Millipore, Burlington, MA) with ChemiDoc Imager (Bio-Rad, Hercules, CA). Non-transfected cell membrane-coated NPs were used as a control.

2.9. Drug loading efficacy and in vitro drug release profile

To determine loading efficacy, Cisplatin encapsulated in PLGA NPs was measured using a UV-VIS Spectrophotometer incorporating the ortho-phenylene diamine (OPDA) technique [60]. The supernatant solution obtained after ultracentrifugation of NPs during the formulation process was used for loading efficiency determination via an indirect method. For the drug release studies, suspensions of Cisplatin-loaded NPs in PBS (pH 7.2) were added to dialysis bags (Spectrum Laboratories, Rancho Dominguez, CA) with a molecular weight cut-off of 8000 Da. Dialysis against PBS was carried out at 37 °C up to 21 days. At pre-determined time points, dialysate was collected and stored at −20 °C for analysis. As described by Mohit et al., [60] dilutions of sample were made using 1 mL of 1.4 mg/mL of OPDA solution (Sigma Aldrich, St. Louis, MO) and 2 mL of phosphate buffer pH 6.8 and heated at 100 °C for 10 min to get a light-green color solution. The solution was cooled, and the volume was adjusted to 10 mL by DMF. The concentration of Cisplatin was then measured using an absorbance spectrometer at λ706 nm. A standard curve was plotted by measuring the absorbance of known concentrations of Cisplatin. The amount of Cisplatin released was then determined against the standard curve and was correlated to the Cisplatin loading efficiency, which was determined using the formula given below.

$$\%\ \text{Loading efficiency} = \frac{\text{Total Cisplatin used} - \text{Cisplatin in supernatant}}{\text{Total Cisplatin used}} \text{X } 100 \quad (1)$$

2.10. Biocompatibility studies

2.10.1. Hemocompatibility

Human blood from healthy donors was collected and handled by the following methods. Informed consent was obtained from the study participants before drawing blood. After collection, human blood was incubated with CAR-T-MNPs at different concentrations (0, 250, 500, 750, and 1000 μg/mL), 0.9% saline (negative control), or distilled water (positive control) for 2 h. Following centrifugation at 1000g, absorbance readings were taken at λ540 nm. The percentage of hemolysis was calculated using the equation below:

$$\%\ \text{Hemolysis} = \frac{(\text{sample OD} - \text{negative control OD})}{(\text{positive control OD} - \text{negative control OD})} \text{X } 100 \quad (2)$$

To study blood clotting kinetics, CAR-T-MNPs of varying concentrations (0, 250, 500, 750, and 1000 μg/ml) were added to blood that was activated with CaCl2. At pre-determined time points (10, 20, 30, and 60 min), the red blood cells (RBCs) not involved in clot formation were lysed. Absorbance readings of supernatant were taken at 540 nm. The absorbance readings were inversely proportional to clot formation.

2.10.2. Cytocompatibility

AT1 cells were seeded (5×10^3 cells/well) in 96-well plates and incubated overnight at 37 °C. CAR-T-MNPs were added at concentrations ranging from 0 to 1000 μg/mL to the seeded cells. After incubation for 48 h, cells were incubated with the MTS reagent (Promega, Madison, WI) for 1 h, followed by absorbance measurement at 490 nm using an UV–Vis spectrophotometer (Tecan, Männedorf, Switzerland). Cell viabilities were calculated via normalizing to the control group (cells exposed to complete media only were considered having a 100% viability).

2.11. Targeting ability of CAR-T-MNPs

For fluorescent uptake microscopy imaging studies, A549 Wildtype (WT) and A549 HER2 KO cells were seeded on glass-bottomed six-well tissue culture plates (Corning, Corning, NY). Coumarin-6 (fluorescent dye)-loaded Jurkat-T-MNPs, PLGA NPs or CAR-T-MNPs were added and incubated with cells for 30 min at 37 °C. Cells were then washed using PBS and were fixed using 5% formaldehyde for 20 min. The cell nuclei were stained using NucBlue (Invitrogen, Waltham, MA), and cells were imaged using the EVOS Floid inverted fluorescent microscopy (Invitrogen, Waltham, MA). For the spectrophotometric analysis of uptake, Coumarin-6 (fluorescent dye) loaded Jurkat-T-MNPs, PLGA NPs and CAR-T-MNPs at different NP concentrations (100 μg/mL, 250 μg/mL, and 500 μg/mL) were exposed to cells in 96-well plates for 30 min and subsequently washed with 1X PBS and lysed with 250 μL/well of 1% Triton® X-100 (30 min incubation). Cell extracts were then analyzed for protein content using the Pierce BCA protein assay kit (Thermo Scientific, Rockford, IL) and Coumarin-6 fluorescent intensity (emitted from particles the cell uptakes) using λ458 nm/540 nm (em/ex) values on a multimode microplate reader (Tecan, Männedorf, Switzerland). Total protein concentration in each lysate was calculated using a BSA standard curve. The uptake of NPs was calculated by normalizing particle concentration (determined from fluorescence intensity in the lysate) in each sample with total cell protein, which correlated to the number of cells in the sample.

2.12. In vitro cell viability MTS assays

A549 WT, A549 HER2 KO and SKOV-3 cells were seeded (5×10^3 cells/well) in 96-well plates and incubated overnight at 37 °C. Free Cisplatin, Cisplatin-loaded PLGA NPs, Jurkat-T-MNPs, and CAR-T-MNPs were then added to the seeded cells (n = 4) at a final Cisplatin concentration of 7 μM (A549), 4 μM (SKOV-3) & 7 μM (A549 HER2 KO). The IC-50 for each cell line was chosen from established literature. The cells were treated for 48 h with the NPs at 37 °C. The absorbance at λ490 nm was measured using a multimode microplate reader (Tecan, Männedorf, Switzerland) after treating with MTS reagents. Cell viabilities were calculated via normalizing to the control group (cells exposed to complete media, 100% viability).

2.13. Animal model

Nude mice (NU/J) aged 5–6 weeks (both sexes) were purchased from Jacksons Laboratory. Briefly, 2×10^6 A549 cells in 200 μL of Matrigel (Corning, Corning, NY) were injected subcutaneously in athymic nude mice. Tumor volumes were checked at regular intervals of three days, and treatment started when the volume reached ~300 mm^3. Tumor volumes were measured using a standard Vernier Caliper. All procedures involving experimental animals were performed in accordance with the protocols approved by the University of Texas at Arlington Institutional Animal Care and Use Committee.

2.14. In vivo biodistribution of CAR-T-MNPs

The biodistribution study was performed to evaluate targeting efficiency of intravenously injected CAR-T-MNPs towards subcutaneous tumors implanted in nude mice. Indocyanine green (ICG)-loaded CAR-T-

MNPs were prepared in the same aforementioned formulation procedure. Saline, ICG-loaded PLGA NPs, Jurkat-T-MNPs, and CAR-T-MNPs were intravenously given to mice via the tail vein at 5 mg of dye (ICG)-loaded particles. At 1, 4, and 8 h, images of animals for all groups were monitored and recorded by the Kodak FX/Pro imaging system. The mice were euthanized at the end time point, and the tumor tissue and major organs were collected, weighed, and fixed with 4% paraformaldehyde. Fluorescence signals of tumors and each organ were recorded using the Kodak FX/Pro imaging system for quantification. Furthermore, weighted tumors and organs were homogenized for 2 min using a tabletop Precellys homogenizer (Bertin Instruments, Montigny-le-Bretonneux, France). Homogenates were centrifuged at 4000 rpm for 10 min, and fluorescent measurements of supernatant's were taken at λ786/825 nm (ex/em) using a multimode microplate reader (Tecan, Männedorf, Switzerland). Effective NP accumulation amounts in all organs and tumors (μg NP per mg of organ) were determined using a standard curve of ICG PLGA NPs and normalized against the saline group.

2.15. In vivo therapeutic efficacy of CAR-T-MNPs

Xenograft tumors as described above were used to evaluate the therapeutic efficacy of CAR-T-MNPs. After the tumor reached ~300 mm^3, mice were randomly distributed into three groups (n = 4). Prior to treatment, all mice were ear-tagged, the initial tumor volumes were measured by a caliper, and body weights were recorded. The treatment groups received a single tail-vein IV administration of either 200 μL of saline (control), Jurkat-T-MNPs, or CAR-T-MNPs. Tumor volume was measured every 2–3 days via a caliper. Tumor volumes were calculated by measuring the tumor perpendicular diameters with a caliper and determined using the formula below, where a and b are the longest diameter and its longest perpendicular diameter, respectively.

$$Tumor\ Volume\ (V) = \frac{a\ x\ 2b}{2} \quad (3)$$

Tumor growth was monitored until the longest diameter reached 20 mm, or the animals exhibited unusual behavior, at which point they were euthanized via carbon dioxide. Tumor tissue was collected and fixed with 4% paraformaldehyde after the mice were euthanized. The tissue was embedded in paraffin wax and sectioned into 5 μm sections using Shandon Finnesse ME microtome (ThermoFisher, Waltham, MA), followed by further histological examination using hematoxylin and eosin (H&E) staining (Abcam, Waltham, MA).

2.16. In vivo toxicity analysis of CAR-T-MNPs

The mice were sacrificed after the completion of the study, and organs from different animal groups were collected and analyzed via histological staining to determine the organ toxicity. The kidneys and lungs from the mice were embedded with paraffin, and then were sliced into 6 μm sections. The lung sections were stained with Masson trichrome stain (StatLab, USA) according to the manufacturers' instructions.

For immunohistochemical staining of the kidney, paraffin sections were rinsed with Tris -Buffered Saline (TBS) and antigen was retrieved by a sodium citrate buffer treatment under steam for 10 min. After subsequent washes with TBS, endogenous peroxidase activity of tissues was abolished by treatment with 0.3% H_2O_2 for 30 min. Following several rinses with TBS, sections were blocked with 5% normal goat serum in TBS for 1 h. Subsequently, the tissue was incubated with anti-Ki67 monoclonal antibody (Abcam, US) overnight. Next, the sections were extensively rinsed with TBS and processed with highly purified Goat-anti-rabbit IgG- FITC labeled secondary antibody (Abcam, US) for 1 h. Following several rinses with TBS, the sections were incubated with DAPI staining (Molecular Probes, US) for nuclei and washed and mounted with mounting media. The cover slip was put on top of mounting media and viewed under 40X in an Echo fluorescent microscope (Echo, San Diego, CA).

2.17. Statistical analysis

GraphPad Prism 9 (GraphPad Software Inc., San Diego, CA) was used to perform statistical analysis. Two-way ANOVA with Tukey's multiple comparisons test was done for all the analyses. Triplicate samples were used for all the studies if not specified. (*P < 0.05, **P < 0.01, ***P < 0.001, ****P < 0.0001). Two-way ANOVA with Dunnett's multiple comparisons test was performed for the tumor growth delay study. A Mantel-Cox test was performed for the mice survival study.

3. Results and discussion

3.1. Generation of CAR-T cells

Plasmids were transfected into Lenti-X 293T cells via Lipofectamine™ 3000 transfection reagent with a high efficiency and evaluated using red fluorescence of mCherry reporter proteins. Transduction efficacy determined through internal mCherry expression showed a distinctive shift in transduced Jurkat T-cells compared to non-transduced cells (Fig. 2A).

As shown in Fig. 2B, Jurkat T-cells were successfully transduced to express anti-HER2 CAR scFv on their membrane surface. The c-myc tag included towards the end of the extracellular CAR construct was used for sorting and CAR characterization. After staining for the c-myc tag with a specific APC-labeled antibody, a distinctive shift was seen in the transduced T-cell group compared to the non-transduced group. In total, approximately 40–50% of the transduced cell population was found to express anti-HER2 CAR receptor on the surface.

Jurkat-transduced cells were sorted using anti-c-myc tag antibody in a FACSMelody™ (BD Biosciences, San Jose, CA) cell sorter with a final yield of 70–80% positive CAR-T cells (Fig. 2). A stability study of sorted CAR-T Jurkat cells was assessed for two weeks, which revealed that 93–97% of CAR-T cells maintained engineered CAR expression. The observed transduction efficiency is comparable to that observed in literature [51]. After the confirmation of engineered CAR T-cells, they were further cultured for isolating of their cell membranes as needed.

3.2. Synthesis and physiochemical and biomimetic characterization of CAR-T-MNPs

The average diameter of the final Cisplatin-loaded CAR-T MNPs was about 195 nm with a polydispersity index (PDI) = 0.117. These NPs were spherical in shape (Fig. 3A). The zeta potential of both extruded and bare PLGA NPs ranged from −7 to −5 mV (Fig. 3B). In recent studies, Wang et al. showed identical results where T-cell membranes coated on nanoparticles displayed a range of −5 to −7 mV[61]. The increase in zeta potential results corresponds to an increase in stability and circulation time of nanoparticles in the blood stream which coincides with the findings in literature [62,63]. The size of the CAR-T-MNPs was ~195 nm, with a nearly 25 nm increase compared to the bare PLGA NPs (~170 nm) (Fig. 3B). The increase in size from coating is comparable to previous studies done by Ma et al. [64] where the T cell membrane was used to coat silica NPs for use as a theranostic drug delivery system. Transmission electron microscopy (TEM) images of CAR-T MNPs revealed a core shell structure of the particle with a size correlating to the DLS data (Fig. 3A). Low polydispersity shows that the particles were homogenous. The loading efficiency of CAR-T-MNPs was about 61%, and the drug release kinetics displayed an initial burst release followed by a sustained release of up to four days of incubation at 37 °C in PBS (pH = 7.4) (Fig. 3C).

Coumarin-6 was loaded inside NPs for locating them in flow cytometry (Green channel). After extrusion, membranes were stained with lipophillic DiD dye (Invitrogen, Waltham, MA) to detect CAR-T

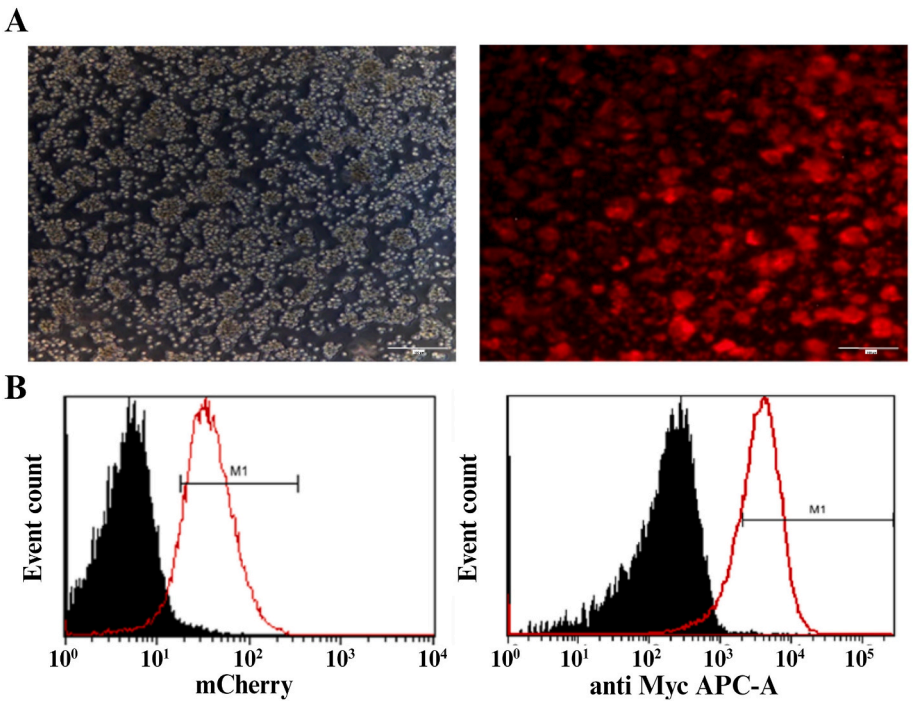

Fig. 2. Confirmation of anti-HER2 scFv transduction on Jurkat T-cells by: **A)** Fluorescent microscopy imaging of mCherry expression on the transduced and sorted cells' brightfield channel (left) and fluorescent channel (right), (scalebar – 100 μm). **B)** Flow cytometric confirmation of Jurkat T-cell transduction, where anti-HER2 CAR transduced cells (red) show a distinctive shift against both mCherry and c-myc tag compared to the non-transduced Jurkat cell (black).

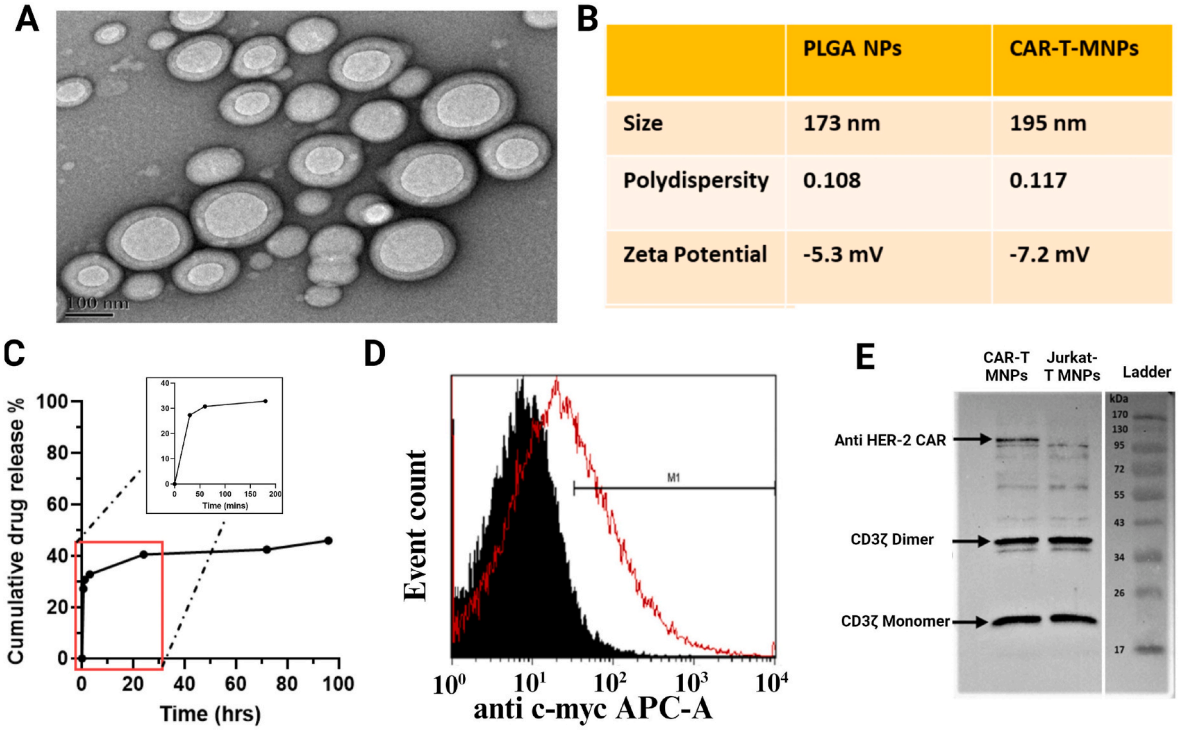

	PLGA NPs	CAR-T-MNPs
Size	173 nm	195 nm
Polydispersity	0.108	0.117
Zeta Potential	-5.3 mV	-7.2 mV

Fig. 3. Physiochemical characterization of CAR-T-MNPs. **A)** TEM image of CAR-T-MNPs. **B)** Size, zeta potential, and polydispersity chart of NP formulations. **C)** Drug release kinetics of CAR-T-MNPs in PBS buffer. Anti-HER2 presence and functionality confirmation of: **D)** CAR-T-MNPs by flow cytometry against c-myc tag protein (CAR-T-MNPs (red) and uncoated PLGA NPs (Black)). **E)** CAR-T-cells by Western Blot shows a distinctive band correlating to anti-HER2 CAR scFv for CAR-T cells. No such band was observed for Jurkat-T-cells. (Number of replicates, n = 3).

membrane (Red channel) presence on the NPs using flow cytometry. Based on flow cytometric data, the coating efficacy of Coumarin-6 PLGA NPs with cell membranes was between 72 and 77% on both transduced and non-transduced CAR-T-cell membrane extruded groups. Furthermore, coating confirmation of PLGA NPs with CAR-T-cell membranes was assessed via fluorescent microscopy. In the merged channel, yellow-

colored particles detected by DiD staining (red) of lipids on the CAR-T membrane coating and Coumarin-6 dye (green) from core PLGA NPs confirms coating of the NPs with cell membranes.

Additionally, we performed flow cytometry using an APC-labeled antibody targeting c-myc tag to re-confirm the presence of HER2 CAR on the extruded NP surface. The results showed a distinctive shift (55–60% positivity) for CAR-T membrane-coated PLGA NPs when compared to that of the non-transduced T-cell membrane NP group (Fig. 3D). Western Blot analysis of isolated CAR-T membranes also showed bands respective to both CD3 and anti HER2 CAR proteins. The estimated size of the anti-HER2 CAR receptor was 89 kDa (Fig. 3E). However, Western Blot results indicated that the band belonging to the receptor appeared on the 105–110 kDA band interval. This increment is attributed to the CAR receptor's glycosylation pattern during post translational modification. As all proteomic scientists certify this phenomenon, glycosylation of the proteins increases their molecular weight. Therefore, it increases the size and slows protein migration down on Western Blot [65]. The respective CD3 zeta chain (housekeeping protein) on the blot is shown as two subsequent bands. The first band appears on 18 kDa, and the other one is around 38 kDa. This indicates that the antibody used in the study recognizes both monomer and homodimer forms of the CD3 zeta receptors. Thus, anti-HER2 CAR protein presence on isolated cell membranes was confirmed (Fig. 3E). Overall, CAR-T-MNP formulation processes were optimized to obtain engineered cell membrane-coated NPs.

3.3. Hemocompatibility and cytocompatibility of CAR-T-MNPs

To test the hemocompatibility of CAR-T-MNPs, their hemolysis and blood clotting properties were investigated. The extruded NPs were hemocompatible since CAR-TMNP-induced hemolysis was measured to be <5% even up to 1000 μg/mL concentration of NPs (Fig. 4). According to the criterion in the ASTM E2524-08 standard, percent hemolysis >5% is considered toxic to red blood cells (ASTM E2524-08, 2013). Thus, CAR-T-MNPs showed complete compatibility for all concentrations. The effects of CAR-T-MNPs on blood clotting were also tested and found to have no significant effects on clotting up to 1000 μg/mL when compared to the 0.9% saline control (Fig. 4). In order to meet the criteria for hemocompatibility, a material must not trigger any thrombogenic or anti-coagulating reactions within the body [66]. Our comprehensive investigation was designed to evaluate how CAR-T-MNPs interacted with the complex dynamics of blood clotting. The results of our study unequivocally demonstrated that CAR-T-MNPs did not elicit any significant alterations in the intricate processes associated with blood clotting.

Cytocompatibility of CAR-T-MNPs was analyzed via a survival analysis study against AT1 healthy lung cells. Various concentrations ranging from 0 to 1000 μg/mL were used for 48-h treatment analysis. CAR-T-MNPs showed very minimal toxicity for concentrations ≤250 μg/mL. The relative toxicity observed in our study at higher concentrations (500 and 1000 μg/mL) might be the result of gas and nutrient exchange prevention due to excessive NP amount in a static 2D cell culture model (Fig. 4C) [67–69]. Moreover, the above mentioned higher concentrations fall far away from the possible physiological desired concentrations of the NPs. These findings are particularly noteworthy as they underscore the safety and suitability of CAR-T-MNPs for potential medical applications, emphasizing their compatibility with the circulatory system.

3.4. Cell uptake and therapeutic efficacy of CAR-T-MNPs in vitro

The targeting efficiency of the CAR-T-MNPs was analyzed *in vitro* by uptake studies (Fig. 5). Briefly, HER2-expressing A549 WT lung cancer cells were used to measure CAR-T-MNP uptake efficiency compared to PLGA NPs and Jurkat-T-MNPs. The confirmation of HER2 protein KO was also verified by flow cytometry. Coumarin-6 loaded PLGA NPs

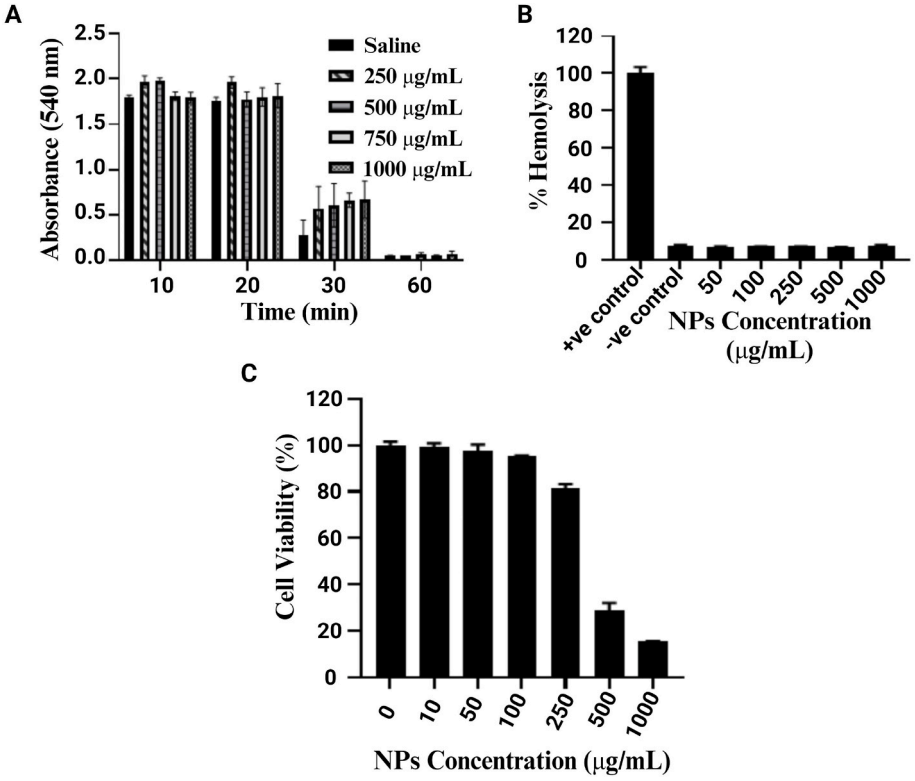

Fig. 4. Hemo- and cyto-compatibility of CAR-T-MNPs *in vitro*. **A)** Blood clotting effect of CAR-T-MNPs at different concentrations (250 μg/mL −1000 μg/mL). **B)** Hemolysis analysis of blood incubated with different concentrations (0 μg/mL - 1000 μg/mL) of CAR-T-MNPs. **C)** Cytocompatibility analysis of CAR-T-MNPs on AT1 cells to determine their *in vitro* cytotoxic effect on different concentrations (0 μg/mL −1000 μg/mL). (Number of replicates, n = 3).

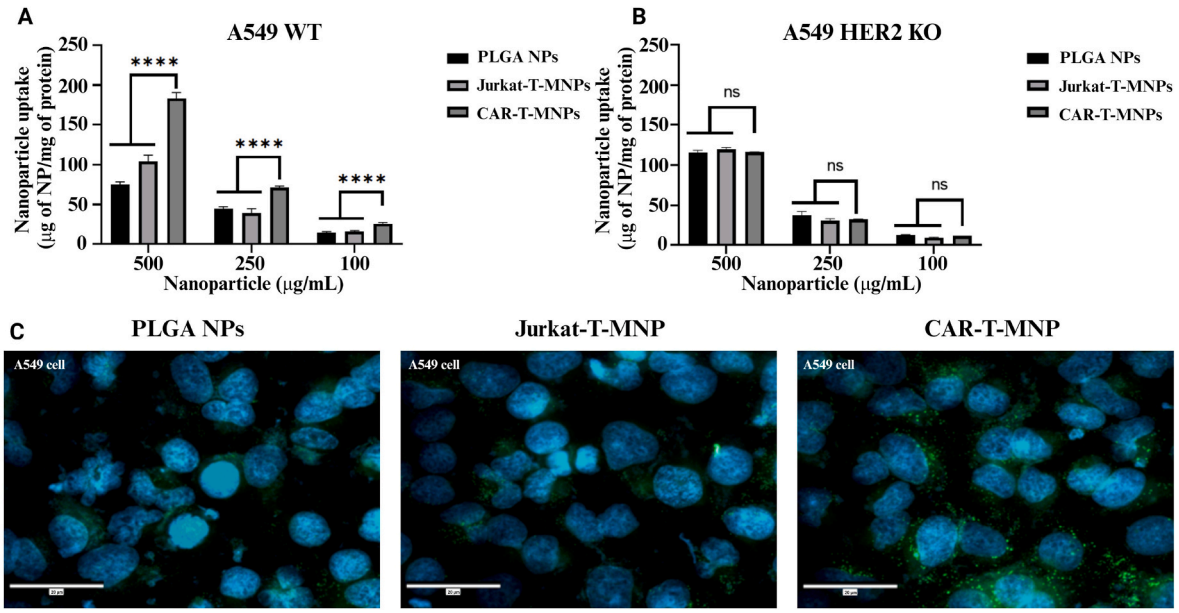

Fig. 5. Spectrophotometric analysis of different NP groups' uptake trend in: **A)** HER2-expressing A549 WT cells and **B)** A549 HER2 KO cells. **C)** Fluorescent uptake images of PLGA NPs, Jurkat-T-MNPs, and CAR-T-MNPs by A549 cells (500 μg/mL), NPs (green) and Nuclei (cyan). The data are shown as mean ± SD (Number of replicates, n = 4, ***P < 0.001, ****P < 0.0001).

coated with either CAR-T-MNPs or Jurkat-T-MNPs were incubated for 30 min with A549 cells. The cells were washed and imaged using a fluorescent microscope. Microscopy images of cells after incubation (Fig. 5C) indicated that anti-HER2 CAR-T-MNPs had a significantly higher uptake by A549 cells compared to those of the Jurkat-T-MNPs or PLGA NPs. Spectrophotometric analysis of the NPs' uptake-exposed cell lysates also revealed that CAR-T-MNPs had a significantly higher uptake by A549 WT cells compared to the other groups (Fig. 5A) for a range of concentrations from 100 to 500 μg/mL. The uptake of CAR-T-MNPs was two-fold higher among comparison groups. Literature has also shown immune cell coated nanoparticles have increased targeting towards inflamed and/or carcinogenic cells [70]. In a recent study, engineered T-cells against glioblastoma showed selective uptake by the target glioblastoma cells. Interestingly, there was no significant nanoparticle uptake by healthy astrocytes. This study also observed a 2.5 fold increase in uptake in glioblastoma cells by the engineered nanoparticles compared to that of non-engineered membrane coated nanoparticles [61].

Thus, the correlating microscopy and spectroscopy studies prove our hypothesis that the functional anti-HER2 molecule on the CAR-T-MNPs significantly enhanced its cancer targeting and uptake onto lung cancer cells and tumors. To verify that the increase in uptake was due to the targeting effect but not to other factors, similar experiments were conducted on HER2-negative A549 HER2 KO cells, and we observed no significant difference in uptake of NPs between CAR-T-MNPs, Jurkat-T-MNPs, and PLGA NPs (Fig. 5B). However, though not significant, we observed that there is a higher uptake of PLGA NPs compared to the Jurkat-T-MNPs in both cell lines; this can likely be either due to the smaller size of PLGA NPs, or the interaction between the cancer cell membrane and NP membrane coating. This, however, further attests the importance of the targeting ligands and their effectiveness in selectively targeting HER2 positive cancer cells.

In vitro cancer killing efficacy was determined by cytotoxicity analysis on HER2-positive A549 WT, SKOV-3 cancer cell lines, and HER2-negative A549 HER2 KO cancer cell lines at specific concentrations. The IC_{50} (half maximal inhibitory concentration) value of Cisplatin on cell lines was chosen from the literature [71–73] to be 7.5 μM, 4 μM, and 7.5 μM (~100, 53, and 100 μg of NPs), respectively. Bunn et al. [74] previously described HER2 expression levels of various NSCLC cell lines via different methods, and found that the A549 cell line expresses moderate to high expression of HER2 protein even if it does not contain gene amplification [74]. The cancer killing efficacy of the CAR-T-MNPs was tested through cell viability assays after 48 h of exposure (Fig. 6A and B). We observed that CAR-T-MNPs showed significantly higher cancer killing efficacy in both HER2-positive cell lines compared to all the other comparison groups. This result demonstrates the effect of CAR-T-MNPs' higher uptake on HER2-expressing cells compared to free drug or uncoated NPs. Jurkat-T-MNPs, however, have a significantly lower cancer killing efficacy compared to CAR-T-MNPs; this shows that NPs' transport into cells are not just passive diffusion or membrane fusion, but rather an active targeting-based killing. Similarly, efficient killing profiles using T-cell membrane-coated NPs have been reported previously, showing the influence of the T-cell membrane in improved endocytosis and release of cargo intracellularly [75,76]. To further prove this effect, we observed that there was no significant difference in cancer killing between the groups in the HER2-negative cancer cell line. We observed no significant difference between Jurkat-T-MNPs and CAR-T-MNPs with similar treatment doses in the HER2-negative cancer cell line. After 4 h of incubation, the cells undergo a washing process to remove any nanoparticles (NPs) that have not been internalized during this time frame. This phenomenon clarifies why CAR-T-MNPs exhibit a more pronounced effect in wild-type (WT) cells compared to HER2-negative cancer cells, as they are taken up via HER-2 dependent targeting. These results indicate that the proposed CAR-T membrane--coated NPs could potentially be used as a targeted chemotherapeutic carrier to effectively treat lung cancer.

3.5. *In vivo targeting efficacy evaluation of CAR-T-MNPs*

The *in vivo* targeting efficacy of CAR-T-MNPs was analyzed by a biodistribution study on a tumor-bearing mouse model. PLGA NPs were loaded with ICG dye for deep-tissue imaging and then coated with either anti-HER2 CAR-T-cells or Jurkat cell membranes. To ascertain whether CAR-T-MNPs could efficiently target, localize, and accumulate at tumor sites, their biodistribution in a HER2-expressing tumor xenograft mouse model was assessed (Fig. 7A). All the groups had NPs accumulated mainly in the liver and spleen within 1 h. However, PLGA NPs gradually cleared from systemic circulation and all organs, including tumors,

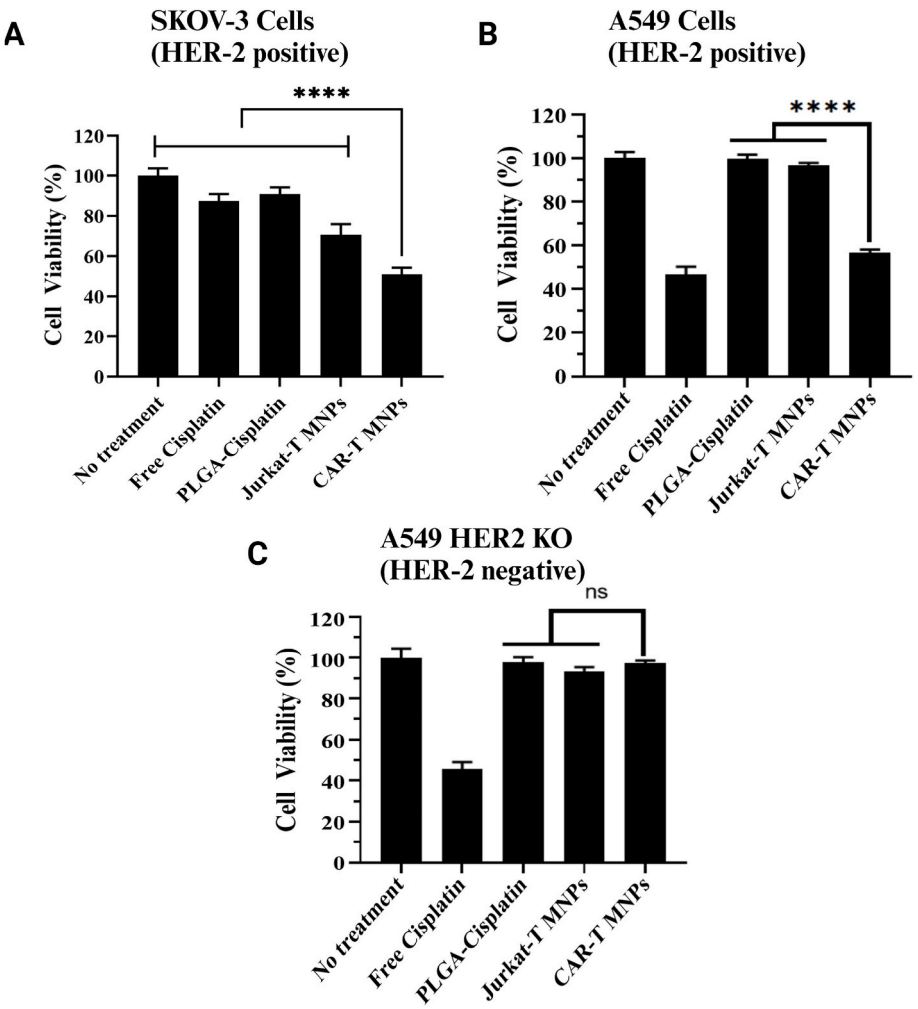

Fig. 6. *In vitro* therapeutic efficacy (cell killing) properties of CAR-T-MNPs. **A)** SKOV-3 **B)** A549 **C)** A549 HER2 KO cells exposed to free Cisplatin, PLGA NPs, Jurkat-T-MNPs & CAR-T-MNPs for 48 h. Cell viability was quantified via MTS assays after exposure (Number of replicates, n = 4, ****P < 0.0001).

without any signs of specific targeting towards the tumor (Fig. 7A). On the other hand, CAR-T-MNP groups showed gradual increases of fluorescence in tumors over the course of study, and slowly cleared from the body after 8 h (Fig. 7A). This increase in accumulation can be attributed to long circulation times without much clearance due to several proteins on the CAR-T-cell membrane coating which aid in immune evasion [64,77].

Tumor accumulation properties of cytotoxic lymphocyte T-cells are especially evident through our results, showing how membrane proteins play a major role in improving targeting of conventional NPs such as PLGA NPs and silica NPs [56,64]. Engineered T-cell membranes, with various targeting proteins such as chimeric antigenic receptors, T-cell receptor complexes, and ScFv can recognize neoantigens from an individual cancer cell and can improve payload drug targeting when used as a platform for personalized medicine in developing this technology [46,51,61,78]. Intensities from the implanted tumors also showed a similar trend in the *in vivo* images. As shown in the *ex vivo* organ and tumor images, all groups showed similar accumulation in the kidney and liver, but when comparing the tumor tissue, CAR-T-MNPs showed significantly higher accumulation compared to those of either Jurkat-T-MNPs or PLGA NPs. Spectrophotometric analysis of lysed organs showed a similar trend of both *in vivo* and *ex vivo* measurements (Fig. 7B). In the kidney and heart, membrane-coated NPs showed lower accumulation compared to the PLGA NP group. In the liver and spleen, despite a trend of low accumulation of membrane-coated groups, the amount of particle per milligram of organ remained relatively similar in all groups. In the kidney, heart and lungs, CAR-T-MNPs showed similar or low levels of accumulation compared to the PLGA NPs and Jurkat-T-MNPs groups, although no statistical significance was observed. Lastly, when tumor accumulation was compared, CAR-T-MNPs had significantly higher accumulation in the tumor tissue (2.3 μg of particle/mg of tumor tissue) compared to that of both the Jurkat-T-MNPs and bare PLGA NPs group (0.21 and 0.46 μg of particle/mg of tumor tissues, respectively) (Fig. 7C). Our results, therefore, show the significant enhancement of CAR-T-MNPs in tumor targeting and accumulation. The CAR-T-MNPs will thus act as a viable carrier for treatment of HER2-expressing lung tumors.

3.6. *In vivo* therapeutic efficacy of CAR-T-MNPs

The *in vivo* therapeutic effect of CAR-T-MNPs was analyzed using a tumor delay growth study in A549 tumor-bearing nude mice in which the anti-tumor effect of CAR-T-MNPs was compared to that of Jurkat-T-MNPs, free Cisplatin and saline (Fig. 8). Groups were chosen based on *in vitro* data with consideration of the main scope of this research. The Cisplatin concentration for all the groups was equal (3 mg/kg). We observed that after two weeks post-treatment, CAR-T-MNPs had a significant reduction in tumor volume growth compared to that of Jurkat-T-MNPs and free Cisplatin (Fig. 8A). Although the tumor growth volumes are not significantly different between free Cisplatin and CAR-T-MNPs groups (Fig. 8A), the CAR-T-MNPs did show better animal survival rate (Fig. 8B) and lower tumor growth compared to that of free

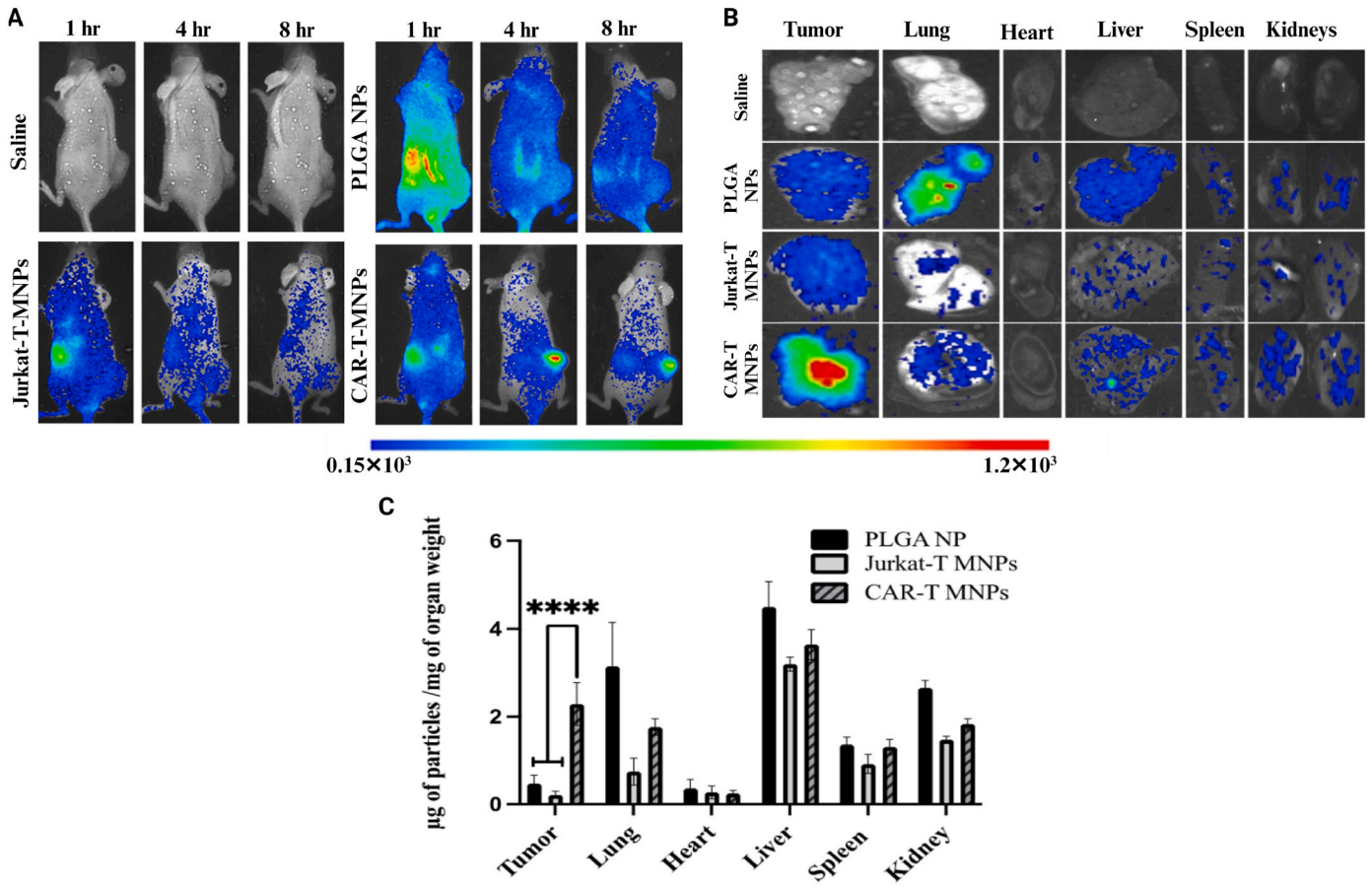

Fig. 7. *In vivo* biodistribution (targeting efficiency) studies. **A)** *In vivo* measurement of average color intensity of tumors/mm2 area on animal groups (CAR-T-MNPs, Jurkat-T-MNPs, PLGA NPs). **B)** Representative *ex vivo* organ images of all biodistribution study groups. **C)** Accumulation efficiency of fabricated nanoparticle systems in individual organs and tumors. (Number of replicates, n = 4, ****P < 0.0001).

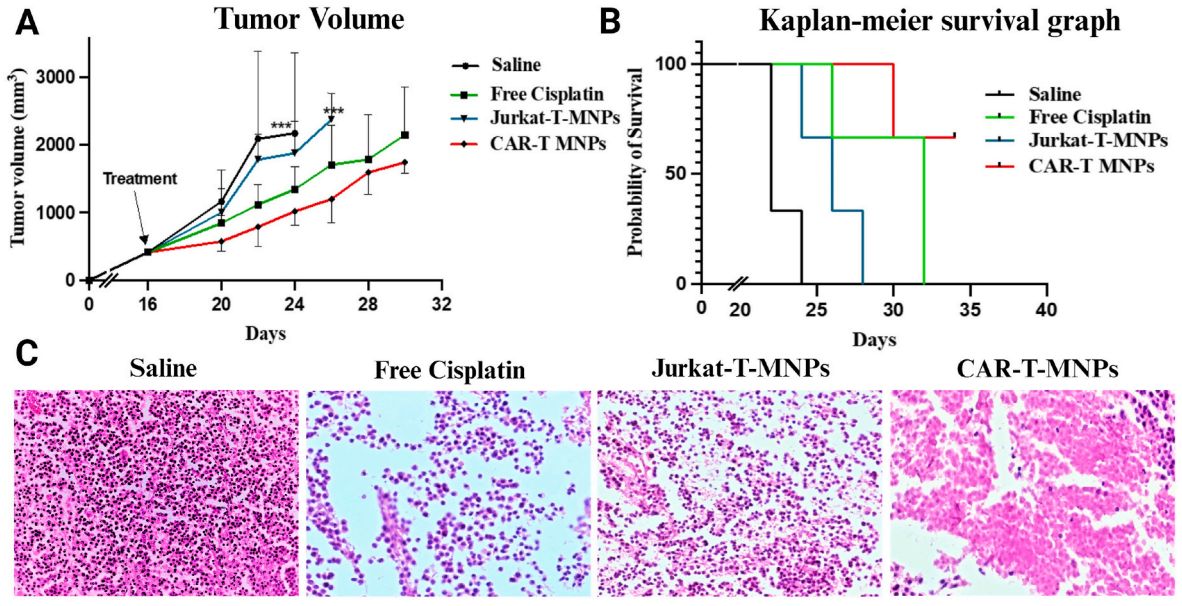

Fig. 8. *In vivo* therapeutic efficacy of CAR-T-MNPs on subcutaneous A549 tumor implanted in nude mice compared to Free Cisplatin, Jurkat-T-MNPs and saline. **A)** Tumor growth delay analysis for 2 weeks after treatment of mice with different groups. **B)** Animal survival analysis of tumor-implanted mice (sacrificed when tumor growth >20 mm in length/width). **C)** Histology analysis (H&E staining) of tumor tissue extracted from mice after experiment endpoint. (Number of replicates, n = 3–6, *P < 0.01).

Cisplatin (Fig. 8A). In addition, the toxicity effects observed in kidneys and lungs for the free Cisplatin group are much higher compared to those of the CAR-T-MNPs group (Fig. 9), indicating the toxicity effects due to non-specific targeting. Though the objective was to compare tumor growth delay for a single dose of NPs (Fig. 8A), the tumor growth delay trend suggests that with multiple doses, the anti-tumor efficacy can be greatly improved for CAR-T-MNPs to the extent of complete tumor regression. The weight change in the mice was also analyzed throughout the duration of the study. We observed no significant changes in the mice's body weight throughout the study for any of the groups. Similar observation regarding the tumor volume growth delay was also supported by the survival of the animals, where we saw significantly higher survival of the CAR-T-MNPs group compared to that of Jurkat-T-MNPs and saline (Fig. 8C).

In vivo anti-tumor effect of the CAR-T-MNPs group was also analyzed by hematoxylin and eosin (H&E) staining of tumor tissues. Histological analysis showed a remarkable killing efficacy in tumor cells for the CAR-T-MNPs-treated group compared to that of other groups and the control. The H&E staining assay also indicated the tumor toxicity of CAR-T-MNPs with decreased cellularity (Fig. 8C). Cells in tumor tissues from the CAR-T-MNPs treatment group were loosely arranged with disintegration, lysed nuclei, and cell fragments, whereas there were only a small number of non-necrotic tumor cells as compared to the control group. There was no obvious organ damage or toxic side effects discovered in any of the groups; however, significant necrosis existed in mouse tumors from CAR-T-MNP- treated groups (Fig. 8C). These results were similar to the observation in the literature for the NP-based cancer therapy mice model for lung cancer [79,80].

Toxicity studies of different animal groups indicated free Cisplatin animal groups showed more toxicity aspects than that of CAR-T-MNPs. Histology study of toxicity in kidneys was performed with staining against known diagnostic ki67 marker, which is upregulated in the acute injury seen in renal tubular cells [81]. The histology staining showed increase ki67 marker expression in free cisplatin group indicating the presence of acute renal injury compared to a very low expression seen in either jurkat or CAR-T cell coated NPs (Fig. 9A and B). We also observed through histological analysis of the lung tissue that CAR-T-MNPs had significantly lower damage to the lung tissue in the form of tissue scarring and collagen deposition (Fig. 9C). With low toxicity and decreased off-target delivery of the drug, CAR-T-MNPs did show a higher survival among all other groups (Fig. 8B), indicative of its high therapeutic value and use against cancer treatment. Furthermore, the off-target delivery of CT drugs or non-targeted NPs loaded with CT drugs can lead to systemic toxicity, adaptive resistance, and, therefore, limited efficacy [82]. Both FDA approved PLGA polymer material and CAR-T-cell membrane-coated groups showed no significant weight change in mice (data not shown), suggesting a low systemic toxicity profile of NPs, which may translate to a very promising drug delivery platform.

Our preliminary research findings thus offer strong support for the promising potential of CAR-T-MNPs as a remarkably precise and efficient tool for targeting cancer cells. It can be clearly noted immunohistochemical staining (Fig. 9A) that cisplatin has a degenerate effect on healthy organs. Though not significant, CAR-T-MNPs had higher tumor regression efficiency, multiple dosed treatment can significantly improve the therapeutic outcome of CAR-T-MNP with low systemic

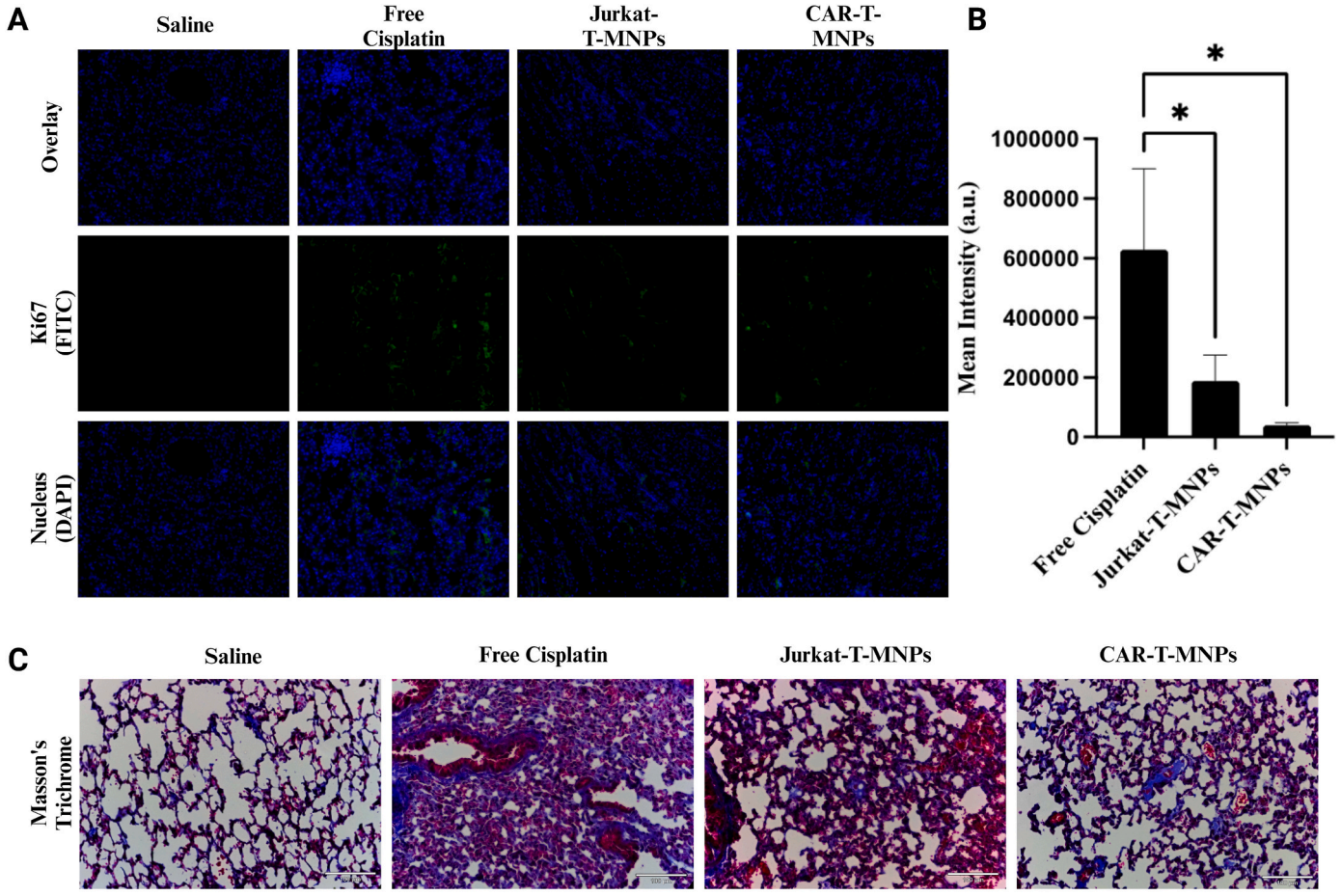

Fig. 9. *In vivo* toxicity analysis of CAR-T-MNPs on subcutaneous A549 tumor implanted in nude mice compared to Jurkat-T-MNPs and saline. **A)** Histological analysis of kidney tissue, immunohistochemistry of Ki67(green) and nucleus (blue). **B)** Quantitative analysis of Ki67 protein expression in kidney tissue. **C)** Masson's trichrome staining of lung tissue comparing tissue scarring/collagen deposition as a result of cisplatin toxicity. (Number of replicates, n = 3, *P < 0.01).

toxicity. Numerous studies have demonstrated the benefits of utilizing multiple doses, emphasizing the low toxicity offered by membrane-coated nanoparticles [83–85]. Although CAR-T based therapy has shown advantages in increasing targeting specificity, combinatorial approach with immuno-therapeutic interventions, immune checkpoint inhibitors and chemotherapeutic interventions needs to be explored for solid tumors. To delve deeper into the capabilities of proposed technology, we plan to conduct more comprehensive investigations using a syngeneic mouse model and human and/or mouse T-cells. This approach will allow us to evaluate the toxicity, targeting precision, and therapeutic effectiveness of primary T-cell membrane-coated MNPs. This innovative strategy holds the promise of extending its application to a broader spectrum of cancers characterized by elevated expressions of specific biomarkers. By doing so, we aim to unlock the full potential of CAR-T-MNPs in the fight against cancer, providing a tailored and effective treatment approach for a variety of malignancies.

4. Conclusion

In summary, we have successfully developed a biomimetic NP platform for targeted treatment of HER2+ lung cancer. The engineered CAR-T-MNPs containing anti-HER2 scFv possess active targeting, tumor accumulation, and therapeutic efficacy as confirmed by our *in vitro* and *in vivo* studies. Therefore, we have proposed and characterized CAR-engineered cell membrane-coated synthetic NPs. Our CAR-T-MNPs displayed a drug encapsulation efficiency of 61% and exhibited sustained drug release over a period of 21 days. The drug release profile was found to be dependent on the existence of a membrane on the particles in which the membrane-coated NPs provided a slower release due to the barrier effect. Fabricated CAR-T-MNPs were shown to be suitable for IV administration in terms of their size (<400 nm), cell compatibility, stability, and hemo-/cyto-compatibility. Moreover, cellular uptake studies showed selective uptake by HER2-positive lung cancer cells when compared to Jurkat membrane-coated PLGA and bare PLGA NPs. These findings also correlated with enhanced therapeutic efficiencies of CAR-T-MNPs. Therefore, a CAR-engineered membrane-coated NP system could be a promising cell-mimicking drug carrier that could improve therapeutic outcomes of lung cancer treatments. On the other hand, severe systemic side effects have always been the major concern of CT drugs. The developed CAR-T technology proved to be an effective and safe alternative. As shown in the pre-clinical results, the CAR-T-MNPs have very high targeting and retention towards tumor tissues and less non-specific organ accumulation. CAR-T-MNP technology also significantly reduced tumor growth with just a single dose treatment.

As cell membrane-coated nanocarriers have great potential to deliver drugs at the desired location, we must also consider the limitations, challenges, and future perspectives associated with this cell membrane approach. The cell membrane is a unique structure and comprised of various molecules (lipids, proteins, receptors, ligands, sugar moieties), some of which are required for targeting (i.e., CAR) and evading immune response (i.e., CD47), while other abundant proteins might have unknown interactions in the host environment. Therefore, more research is needed in the biomimetic drug delivery field to demonstrate its potential in translational research. New CAR-like molecule instruments such as viruses or virus-like particles as carriers, new biosimilars and therapeutic proteins such as payloads inside the carriers and T cell engagers (BiTes), and bispecific antibodies or double-sided antibodies as targeting ligands, might engender new strategies to further develop the biomimetic payload delivery field. As one of these new strategies is under investigation by our lab to implement double-sided chimeric receptors and antibodies into the design, it might be a new way to further develop the existing platform [86]. By continuing this line of research, we expect that fully bioinspired carriers might be designed, developed, and fabricated without human or lab intervention. Therefore, the new generation of drug carriers ready for human use can be fabricated directly either the cell culture (*in vitro*) or inside our bodies by our own cells. Various studies are already underway to improve and optimize the coating efficiency of these membrane to effectively target diseases [87,88].

In conclusion, this proposed research will reach new horizons in design and development of superior therapeutic carrier platforms when compared to existing nanoparticulate systems. Importantly, the development of such personal medicine practices will enable us to improve alternative strategies for other diseases. As a result, the development of biomimetic therapeutic carriers, such as those mentioned in this research, will lead to the emergence of the next generation of targeting and delivery systems by integrating drug delivery systems into biological systems.

Ethical approval

The Animal experiments conducted in the study were approved by Institutional Animal Care & Use Committee (IACUC) under the protocol number #A017.12. There were no human subjects involved in the study.

CRediT authorship contribution statement

Serkan Yaman: Writing – original draft, Visualization, Validation, Software, Methodology, Investigation, Formal analysis, Data curation, Conceptualization. **Harish Ramachandramoorthy:** Writing – review & editing, Writing – original draft, Visualization, Validation, Software, Methodology, Investigation, Formal analysis, Data curation, Conceptualization. **Priyanka Iyer:** Writing – review & editing, Visualization, Validation, Methodology, Investigation. **Uday Chintapula:** Writing – review & editing, Visualization, Software, Methodology, Investigation, Formal analysis. **Tam Nguyen:** Writing – review & editing, Validation, Methodology, Investigation. **Manoj Sabnani:** Visualization, Validation, Methodology, Formal analysis, Data curation. **Tanviben Kotadia:** Methodology, Investigation, Data curation. **Soroush Ghaffari:** Methodology, Investigation. **Laurentiu M. Pop:** Writing – review & editing, Visualization, Methodology. **Raquibul Hannan:** Writing – review & editing, Visualization, Supervision, Resources, Project administration, Investigation, Funding acquisition, Data curation. **Jon A. Weidanz:** Writing – review & editing, Writing – original draft, Validation, Supervision, Project administration, Investigation, Funding acquisition, Data curation, Conceptualization. **Kytai T. Nguyen:** Writing – review & editing, Writing – original draft, Supervision, Software, Resources, Project administration, Investigation, Funding acquisition, Formal analysis, Conceptualization.

Declaration of competing interest

There is no Conflict of Interest. The co-authors have approved the manuscript submission.

Acknowledgements

This work was supported by the Cancer Prevention & Research Institute of Texas (CPRIT) High-Impact/High-Risk Research Awards # RP210206. Figures were generated using Biorender. The manuscript was edited by Sepeadeh Radpour.

References

[1] V.L. Athey, R.J. Suckling, A.M. Tod, S.J. Walters, T.K. Rogers, Early diagnosis of lung cancer: evaluation of a community-based social marketing intervention, Thorax 67 (5) (2012) 412–417.

[2] M. Fukuoka, S. Yano, G. Giaccone, T. Tamura, K. Nakagawa, J.Y. Douillard, Y. Nishiwaki, J. Vansteenkiste, S. Kudoh, D. Rischin, R. Eek, T. Horai, K. Noda, I. Takata, E. Smit, S. Averbuch, A. Macleod, A. Feyereislova, R.P. Dong, J. Baselga, Multi-institutional randomized phase II trial of gefitinib for previously treated patients with advanced non-small-cell lung cancer (The IDEAL 1 Trial) [corrected], J. Clin. Oncol. 21 (12) (2003) 2237–2246.

[3] R. Siegel, D. Naishadham, A. Jemal, Cancer statistics, 2013, CA A Cancer J. Clin. 63 (1) (2013) 11–30.
[4] K. Nurgali, R.T. Jagoe, R. Abalo, Editorial: adverse effects of cancer chemotherapy: anything new to improve tolerance and reduce sequelae? Front. Pharmacol. 9 (2018).
[5] V. Dilalla, G. Chaput, T. Williams, K. Sultanem, Radiotherapy side effects: integrating a survivorship clinical lens to better serve patients, Curr. Oncol. 27 (2) (2020).
[6] T. Sadhukha, T.S. Wiedmann, J. Panyam, Inhalable magnetic nanoparticles for targeted hyperthermia in lung cancer therapy, Biomaterials 34 (21) (2013) 5163–5171.
[7] B. Besse, T. Le Chevalier, Developments in the treatment of early NSCLC: when to use chemotherapy, Ann. Oncol. 23 (Suppl 10) (2012) x52–x59.
[8] M.A. Socinski, J.G. Rosenman, Chemotherapeutic issues in the management of unresectable stage III non-small cell lung cancer, Semin. Oncol. 32 (2 Suppl 3) (2005) S18–S24.
[9] T. Ohguri, H. Imada, K. Yahara, S.D. Moon, S. Yamaguchi, K. Yatera, H. Mukae, T. Hanagiri, F. Tanaka, Y. Korogi, Re-irradiation plus regional hyperthermia for recurrent non-small cell lung cancer: a potential modality for inducing long-term survival in selected patients, Lung Cancer 77 (1) (2012) 140–145.
[10] T. Ohguri, H. Imada, K. Yahara, T. Morioka, K. Nakano, H. Terashima, Y. Korogi, Radiotherapy with 8-MHz radiofrequency-capacitive regional hyperthermia for stage III non-small-cell lung cancer: the radiofrequency-output power correlates with the intraesophageal temperature and clinical outcomes, Int. J. Radiat. Oncol. Biol. Phys. 73 (1) (2009) 128–135.
[11] T. Pho-iam, P. Punnakitikashem, C. Somboonyosdech, S. Sripinitchai, P. Masaratana, V. Sirivatanauksorn, Y. Sirivatanauksorn, C. Wongwan, K. T. Nguyen, C. Srisawat, PLGA nanoparticles containing α-fetoprotein siRNA induce apoptosis and enhance the cytotoxic effects of doxorubicin in human liver cancer cell line, Biochem. Biophys. Res. Commun. 553 (2021) 191–197.
[12] S. Kona, J.-F. Dong, Y. Liu, J. Tan, K.T. Nguyen, Biodegradable nanoparticles mimicking platelet binding as a targeted and controlled drug delivery system, Int. J. Pharm. 423 (2) (2012) 516–524.
[13] R. Domínguez-Ríos, D.R. Sánchez-Ramírez, K. Ruiz-Saray, P.E. Oceguera-Basurto, M. Almada, J. Juárez, A. Zepeda-Moreno, A. del Toro-Arreola, A. Topete, A. Daneri-Navarro, Cisplatin-loaded PLGA nanoparticles for HER2 targeted ovarian cancer therapy, Colloids Surf. B Biointerfaces 178 (2019) 199–207.
[14] S.M. Moghimi, J. Szebeni, Stealth liposomes and long circulating nanoparticles: critical issues in pharmacokinetics, opsonization and protein-binding properties, Prog. Lipid Res. 42 (6) (2003) 463–478.
[15] M.L. Immordino, F. Dosio, L. Cattel, Stealth liposomes: review of the basic science, rationale, and clinical applications, existing and potential, Int. J. Nanomed. 1 (3) (2006) 297.
[16] M. Lundqvist, J. Stigler, G. Elia, I. Lynch, T. Cedervall, K.A. Dawson, Nanoparticle size and surface properties determine the protein corona with possible implications for biological impacts, Proc. Natl. Acad. Sci. USA 105 (38) (2008) 14265–14270.
[17] M.P. Monopoli, D. Walczyk, A. Campbell, G. Elia, I. Lynch, F. Baldelli Bombelli, K. A. Dawson, Physical– chemical aspects of protein corona: relevance to *in vitro* and *in vivo* biological impacts of nanoparticles, J. Am. Chem. Soc. 133 (8) (2011) 2525–2534.
[18] C. Corbo, R. Molinaro, A. Parodi, N.E. Toledano Furman, F. Salvatore, E. Tasciotti, The impact of nanoparticle protein corona on cytotoxicity, immunotoxicity and target drug delivery, Nanomedicine 11 (1) (2016) 81–100.
[19] N. Feliu, D. Docter, M. Heine, P. del Pino, S. Ashraf, J. Kolosnjaj-Tabi, P. Macchiarini, P. Nielsen, D. Alloyeau, F. Gazeau, *In vivo* degeneration and the fate of inorganic nanoparticles, Chem. Soc. Rev. 45 (9) (2016) 2440–2457.
[20] S. Zanganeh, R. Spitler, M. Erfanzadeh, A.M. Alkilany, M. Mahmoudi, Protein corona: opportunities and challenges, Int. J. Biochem. Cell Biol. 75 (2016) 143–147.
[21] H. Yin, R. Chen, P.S. Casey, P.C. Ke, T.P. Davis, C. Chen, Reducing the cytotoxicity of ZnO nanoparticles by a pre-formed protein corona in a supplemented cell culture medium, RSC Adv. 5 (90) (2015) 73963–73973.
[22] V. Escamilla-Rivera, M. Uribe-Ramirez, S. Gonzalez-Pozos, O. Lozano, S. Lucas, A. De Vizcaya-Ruiz, Protein corona acts as a protective shield against Fe3O4-PEG inflammation and ROS-induced toxicity in human macrophages, Toxicol. Lett. 240 (1) (2016) 172–184.
[23] A. Weidner, J. Clement, F. von Eggeling, D. Fischer, C. Gräfe, M. vd Lühe, R. Müller, F. Schacher, S. Dutz, In Formation of a biocompatible protein corona on magnetic nanoparticles, in: Magnetic Particle Imaging (IWMPI), 2015 5th International Workshop on, IEEE, 2015, 1-1.
[24] M. Mahmoudi, Protein corona: the golden gate to clinical applications of nanoparticles, Int. J. Biochem. Cell Biol. 75 (2016) 141–142.
[25] J. Hühn, C. Fedeli, Q. Zhang, A. Masood, P. del Pino, N.M. Khashab, E. Papini, W. J. Parak, Dissociation coefficients of protein adsorption to nanoparticles as quantitative metrics for description of the protein corona: a comparison of experimental techniques and methodological relevance, Int. J. Biochem. Cell Biol. 75 (2016) 148–161.
[26] A. Parodi, R. Molinaro, M. Sushnitha, M. Evangelopoulos, J.O. Martinez, N. Arrighetti, C. Corbo, E. Tasciotti, Bio-inspired engineering of cell-and virus-like nanoparticles for drug delivery, Biomaterials 147 (2017) 155–168.
[27] J.-W. Yoo, D.J. Irvine, D.E. Discher, S. Mitragotri, Bio-inspired, bioengineered and biomimetic drug delivery carriers, Nat. Rev. Drug Discov. 10 (7) (2011) 521.
[28] Y. Barenholz, Sphingomyelin and cholesterol: from membrane biophysics and rafts to potential medical applications, in: Membrane Dynamics and Domains, Springer, 2004, pp. 167–215.
[29] R. Langer, D.A. Tirrell, Designing materials for biology and medicine, Nature 428 (6982) (2004) 487.
[30] D.J. Irvine, M.A. Swartz, G.L. Szeto, Engineering synthetic vaccines using cues from natural immunity, Nat. Mater. 12 (11) (2013) 978.
[31] M. Manchester, P. Singh, Virus-based nanoparticles (VNPs): platform technologies for diagnostic imaging, Adv. Drug Deliv. Rev. 58 (14) (2006) 1505–1522.
[32] T.J. Merkel, S.W. Jones, K.P. Herlihy, F.R. Kersey, A.R. Shields, M. Napier, J. C. Luft, H. Wu, W.C. Zamboni, A.Z. Wang, Using mechanobiological mimicry of red blood cells to extend circulation times of hydrogel microparticles, Proc. Natl. Acad. Sci. USA 108 (2) (2011) 586–591.
[33] G. Von Maltzahn, J.-H. Park, K.Y. Lin, N. Singh, C. Schwöppe, R. Mesters, W. E. Berdel, E. Ruoslahti, M.J. Sailor, S.N. Bhatia, Nanoparticles that communicate *in vivo* to amplify tumour targeting, Nat. Mater. 10 (7) (2011) 545.
[34] C.-M.J. Hu, L. Zhang, S. Aryal, C. Cheung, R.H. Fang, L. Zhang, Erythrocyte membrane-camouflaged polymeric nanoparticles as a biomimetic delivery platform, Proc. Natl. Acad. Sci. USA 108 (27) (2011) 10980–10985.
[35] H. Cao, Z. Dan, X. He, Z. Zhang, H. Yu, Q. Yin, Y. Li, Liposomes coated with isolated macrophage membrane can target lung metastasis of breast cancer, ACS Nano 10 (8) (2016) 7738–7748.
[36] C. Gao, Z. Lin, B. Jurado-Sánchez, X. Lin, Z. Wu, Q. He, Stem cell membrane-coated nanogels for highly efficient *in vivo* tumor targeted drug delivery, Small 12 (30) (2016) 4056–4062.
[37] A.J. Trinidad, S.J. Hong, Q. Peng, S.J. Madsen, H. Hirschberg, Combined concurrent photodynamic and gold nanoshell loaded macrophage-mediated photothermal therapies: an *in vitro* study on squamous cell head and neck carcinoma, Laser Surg. Med. 46 (4) (2014) 310–318.
[38] B. Bahmani, D. Bacon, B. Anvari, Erythrocyte-derived photo-theranostic agents: hybrid nano-vesicles containing indocyanine green for near infrared imaging and therapeutic applications, Sci. Rep. 3 (2013) 2180.
[39] S.-K. Baek, A.R. Makkouk, T. Krasieva, C.-H. Sun, S.J. Madsen, H. Hirschberg, Photothermal treatment of glioma; an *in vitro* study of macrophage-mediated delivery of gold nanoshells, J. Neuro-Oncol. 104 (2) (2011) 439–448.
[40] T.A. Springer, Traffic signals for lymphocyte recirculation and leukocyte emigration: the multistep paradigm, Cell 76 (2) (1994) 301–314.
[41] M. Baggiolini, Chemokines and leukocyte traffic, Nature 392 (6676) (1998) 565.
[42] J. Panés, M. Perry, D.N. Granger, Leukocyte-endothelial cell adhesion: avenues for therapeutic intervention, Br. J. Pharmacol. 126 (3) (1999) 537–550.
[43] K. Ley, Molecular mechanisms of leukocyte recruitment in the inflammatory process, Cardiovasc. Res. 32 (4) (1996) 733–742.
[44] Y. Huang, X. Gao, J. Chen, Leukocyte-derived biomimetic nanoparticulate drug delivery systems for cancer therapy, Acta Pharm. Sin. B 8 (1) (2018) 4–13.
[45] M.J. Mitchell, M.R. King, Leukocytes as carriers for targeted cancer drug delivery, Expet Opin. Drug Deliv. 12 (3) (2015) 375–392.
[46] Yaman, S.; Ramachandramoorthy, H.; Oter, G.; Zhukova, D.; Nguyen, T.; Sabnani, M. K.; Weidanz, J. A.; Nguyen, K. T., Melanoma Peptide MHC Specific TCR Expressing T-Cell Membrane Camouflaged PLGA Nanoparticles for Treatment of Melanoma Skin Cancer. (2296-4185 (Print).
[47] C. von Roemeling, W. Jiang, C.K. Chan, I.L. Weissman, B.Y. Kim, Breaking down the barriers to precision cancer nanomedicine, Trends Biotechnol. 35 (2) (2017) 159–171.
[48] T. Kang, Q. Zhu, D. Wei, J. Feng, J. Yao, T. Jiang, Q. Song, X. Wei, H. Chen, X. Gao, J. Chen, Nanoparticles coated with neutrophil membranes can effectively treat cancer metastasis, ACS Nano 11 (2) (2017) 1397–1411.
[49] L. Zhang, R. Li, H. Chen, J. Wei, H. Qian, S. Su, J. Shao, L. Wang, X. Qian, B. Liu, Human cytotoxic T-lymphocyte membrane-camouflaged nanoparticles combined with low-dose irradiation: a new approach to enhance drug targeting in gastric cancer, Int. J. Nanomed. 12 (2017) 2129.
[50] A. Parodi, N. Quattrocchi, A.L. Van De Ven, C. Chiappini, M. Evangelopoulos, J. O. Martinez, B.S. Brown, S.Z. Khaled, I.K. Yazdi, M.V. Enzo, Synthetic nanoparticles functionalized with biomimetic leukocyte membranes possess cell-like functions, Nat. Nanotechnol. 8 (1) (2013) 61.
[51] Ma, W.; Zhu, D.; Li, J.; Chen, X.; Xie, W.; Jiang, X.; Wu, L.; Wang, G.; Xiao, Y.; Liu, Z.; Wang, F.; Li, A.; Shao, D.; Dong, W.; Liu, W.; Yuan, Y., Coating Biomimetic Nanoparticles with Chimeric Antigen Receptor T Cell-Membrane Provides High Specificity for Hepatocellular Carcinoma Photothermal Therapy Treatment. (1838-7640 (Electronic)).
[52] M. Crittenden, M. Gough, J. Chester, T. Kottke, J. Thompson, A. Ruchatz, T. Clackson, F.L. Cosset, H. Chong, R.M. Diaz, Pharmacologically regulated production of targeted retrovirus from T cells for systemic antitumor gene therapy, Cancer Res. 63 (12) (2003) 3173–3180.
[53] N.E. Toledano Furman, Y. Lupu-Haber, T. Bronshtein, L. Kaneti, N. Letko, E. Weinstein, L. Baruch, M. Machluf, Reconstructed stem cell nanoghosts: a natural tumor targeting platform, Nano Lett. 13 (7) (2013) 3248–3255.
[54] R.H. Fang, C.-M.J. Hu, B.T. Luk, W. Gao, J.A. Copp, Y. Tai, D.E. O'Connor, L. Zhang, Cancer cell membrane-coated nanoparticles for anticancer vaccination and drug delivery, Nano Lett. 14 (4) (2014) 2181–2188.
[55] J.-G. Piao, L. Wang, F. Gao, Y.-Z. You, Y. Xiong, L. Yang, Erythrocyte membrane is an alternative coating to polyethylene glycol for prolonging the circulation lifetime of gold nanocages for photothermal therapy, ACS Nano 8 (10) (2014) 10414–10425.
[56] S. Yaman, U. Chintapula, E. Rodriguez, H. Ramachandramoorthy, K.T. Nguyen, Cell-mediated and cell membrane-coated nanoparticles for drug delivery and cancer therapy, Cancer Drug Resist. 3 (4) (2020) 879–911.
[57] J. Elegheert, E. Behiels, B. Bishop, S. Scott, R.E. Woolley, S.C. Griffiths, E.F. X. Byrne, V.T. Chang, D.I. Stuart, E.Y. Jones, C. Siebold, A.R. Aricescu, Lentiviral

transduction of mammalian cells for fast, scalable and high-level production of soluble and membrane proteins, Nat. Protoc. 13 (12) (2018) 2991–3017.
[58] C. Fernández-Ponce, M.C. Durán-Ruiz, I. Narbona-Sánchez, J.P. Muñoz-Miranda, M.M. Arbulo-Echevarria, A. Serna-Sanz, C. Baumann, R. Litrán, E. Aguado, W. Bloch, F. García-Cozar, Ultrastructural localization and molecular associations of HCV capsid protein in jurkat T cells, Front. Microbiol. 8 (2018).
[59] B.S. Paugh, L. Baranyi, A. Roy, H.-J. He, L. Harris, K.D. Cole, M. Artlip, C. Raimund, P.S. Langan, S. Jana, R.J. Orentas, S. Lin-Gibson, W. Krueger, B. Dropulić, Reference standards for accurate validation and optimization of assays that determine integrated lentiviral vector copy number in transduced cells, Sci. Rep. 11 (1) (2021) 389.
[60] M. Basotra, S.K. Singh, M. Gulati, Development and validation of a simple and sensitive spectrometric method for estimation of cisplatin hydrochloride in tablet dosage forms: application to dissolution studies, ISRN Analyt. Chem. 2013 (2013) 936254.
[61] Wang, W.; Wu, F.; Mohammadniaei, M.; Zhang, M.; Li, Y.; Sun, Y.; Tang, B. Z., Genetically Edited T-Cell Membrane Coated AIEgen Nanoparticles Effectively Prevents Glioblastoma Recurrence. (1878-5905 (Electronic)).
[62] Liu, H. J.; Wang, M.; Shi, S.; Hu, X.; Xu, P., A Therapeutic Sheep in Metastatic Wolf's Clothing: Trojan Horse Approach for Cancer Brain Metastases Treatment. (2150-5551 (Electronic).
[63] Q. Chen, L. Zhang, L. Li, M. Tan, W. Liu, S. Liu, Z. Xie, W. Zhang, Z. Wang, Y. Cao, T. Shang, H. Ran, Cancer cell membrane-coated nanoparticles for bimodal imaging-guided photothermal therapy and docetaxel-enhanced immunotherapy against cancer, J. Nanobiotechnol. 19 (1) (2021) 449.
[64] W. Ma, D. Zhu, J. Li, X. Chen, W. Xie, X. Jiang, L. Wu, G. Wang, Y. Xiao, Z. Liu, F. Wang, A. Li, D. Shao, W. Dong, W. Liu, Y. Yuan, Coating biomimetic nanoparticles with chimeric antigen receptor T cell-membrane provides high specificity for hepatocellular carcinoma photothermal therapy treatment, Theranostics 10 (3) (2020) 1281–1295.
[65] S. Hirobe, K. Imaeda, M. Tachibana, N. Okada, The effects of chimeric antigen receptor (CAR) hinge domain post-translational modifications on CAR-T cell activity, Int. J. Mol. Sci. (2022) [Online].
[66] H. Xu, K.T. Nguyen, E.S. Brilakis, J. Yang, E. Fuh, S. Banerjee, Enhanced endothelialization of a new stent polymer through surface enhancement and incorporation of growth factor-delivering microparticles, J. Cardio. Trans. Res. 5 (4) (2012) 519–527.
[67] J.W. Choi, S.-H. Bae, I.Y. Kim, M. Kwak, T.G. Lee, M.B. Heo, Testing in vitro toxicity of nanoparticles in 3D cell culture with various extracellular matrix scaffold, bioRxiv 2021 (2021), 03.18.436024.
[68] Kapałczyńska, M.; Kolenda, T.; Przybyła, W.; Zajączkowska, M.; Teresiak, A.; Filas, V.; Ibbs, M.; Bliźniak, R.; Łuczewski, Ł.; Lamperska, K., 2D and 3D Cell Cultures - a Comparison of Different Types of Cancer Cell Cultures. (1734-1922 (Print).
[69] S. Behzadi, N.M. Vatan, K. Lema, D. Nwaobasi, I. Zenkov, P.P.S.S. Abadi, D. A. Khan, C. Corbo, H. Aghaverdi, O.C. Farokhzad, M. Mahmoudi, Flat cell culturing surface may cause misinterpretation of cellular uptake of nanoparticles, Adv. Biosyst. 2 (6) (2018) 1800046.
[70] Deng, G.; Sun, Z.; Li, S.; Peng, X.; Li, W.; Zhou, L.; Ma, Y.; Gong, P.; Cai, L. A.-O., Cell-Membrane Immunotherapy Based on Natural Killer Cell Membrane Coated Nanoparticles for the Effective Inhibition of Primary and Abscopal Tumor Growth. (1936-086X (Electronic)).
[71] Kanaani, L.; Javadi I Fau - Ebrahimifar, M.; Ebrahimifar M; Fau - Ebrahimi Shahmabadi, H.; Ebrahimi Shahmabadi; H Fau - Akbarzadeh Khiyav, A.; Akbarzadeh Khiyav A Fau - Mehrdiba, T.; Mehrdiba, T., Effects of Cisplatin-Loaded Niosomal Nanoparticleson BT-20 Human Breast Carcinoma Cells. (2476-762X (Electronic)).
[72] Monroe, J. D.; Hodzic, D.; Millay, M. H.; Patty, B. G.; Smith, M. A.-O., Anti-cancer and ototoxicity characteristics of the curcuminoids, CLEFMA and EF24, in combination with cisplatin. LID - 10.3390/molecules24213889 [doi] LID - 3889. (1420-3049 (Electronic)).
[73] Y. Jiang, J. Jiang, H. Jia, Z. Qiao, J. Zhang, Recovery of miR-139-5p in ovarian cancer reverses cisplatin resistance by targeting C-jun, Cell. Physiol. Biochem. 51 (2018) 129+.
[74] Bunn, P. A., Jr.; Helfrich B Fau - Soriano, A. F.; Soriano Af Fau - Franklin, W. A.; Franklin Wa Fau - Varella-Garcia, M.; Varella-Garcia M Fau - Hirsch, F. R.; Hirsch Fr Fau - Baron, A.; Baron A Fau - Zeng, C.; Zeng C Fau - Chan, D. C.; Chan, D. C., Expression of Her-2/neu in Human Lung Cancer Cell Lines by Immunohistochemistry and Fluorescence in Situ Hybridization and its Relationship to *in Vitro* Cytotoxicity by Trastuzumab and Chemotherapeutic Agents. (1078-0432 (Print)).
[75] Y. Han, H. Pan, W. Li, Z. Chen, A. Ma, T. Yin, R. Liang, F. Chen, Y. Ma, Y. Jin, M. Zheng, B. Li, L. Cai, T cell membrane mimicking nanoparticles with bioorthogonal targeting and immune recognition for enhanced photothermal therapy, Adv. Sci. 6 (15) (2019) 1900251.
[76] M. Kang, J. Hong, M. Jung, S.P. Kwon, S.Y. Song, H.Y. Kim, J.-R. Lee, S. Kang, J. Han, J.-H. Koo, J.H. Ryu, S. Lim, H.S. Sohn, J.-M. Choi, J. Doh, B.-S. Kim, T-Cell-Mimicking nanoparticles for cancer immunotherapy, Adv. Mater. 32 (39) (2020) 2003368.
[77] J. Zhang, H. Tang, Z. Liu, B. Chen, Effects of major parameters of nanoparticles on their physical and chemical properties and recent application of nanodrug delivery system in targeted chemotherapy, Int. J. Nanomed. 12 (2017) 8483–8493.
[78] P. Gong, Y. Wang, P. Zhang, Z. Yang, W. Deng, Z. Sun, M. Yang, X. Li, G. Ma, G. Deng, S. Dong, L. Cai, W. Jiang, Immunocyte membrane-coated nanoparticles for cancer immunotherapy, Cancers 13 (1) (2021).
[79] G.G. Hillman, F. Lonardo, D.J. Hoogstra, J. Rakowski, C.K. Yunker, M.C. Joiner, G. Dyson, S. Gadgeel, V. Singh-Gupta, Axitinib improves radiotherapy in murine xenograft lung tumors, Trans. Oncol. 7 (3) (2014) 400–409.
[80] J.-Y. Zhu, D.-W. Zheng, M.-K. Zhang, W.-Y. Yu, W.-X. Qiu, J.-J. Hu, J. Feng, X.-Z. Zhang, Preferential cancer cell self-recognition and tumor self-targeting by coating nanoparticles with homotypic cancer cell membranes, Nano Lett. 16 (9) (2016) 5895–5901.
[81] Yamashita, N.; Nakai, K.; Nakata, T.; Nakamura, I.; Kirita, Y.; Matoba, S.; Humphreys, B. D.; Tamagaki, K.; Kusaba, T., Cumulative DNA Damage by Repeated Low-Dose Cisplatin Injection Promotes the Transition of Acute to Chronic Kidney Injury in Mice. (2045-2322 (Electronic)).
[82] M.J. Mitchell, M.M. Billingsley, R.M. Haley, M.E. Wechsler, N.A. Peppas, R. Langer, Engineering precision nanoparticles for drug delivery, Nat. Rev. Drug Discov. 20 (2) (2021) 101–124.
[83] Y. Zou, Y. Sun, Y. Wang, D. Zhang, H. Yang, X. Wang, M. Zheng, B. Shi, Cancer cell-mitochondria hybrid membrane coated Gboxin loaded nanomedicines for glioblastoma treatment, Nat. Commun. 14 (1) (2023) 4557.
[84] J.L. Perry, S. Tian, N. Sengottuvel, E.B. Harrison, B.K. Gorentla, C.H. Kapadia, N. Cheng, J.C. Luft, J.P.Y. Ting, J.M. DeSimone, C.V. Pecot, Pulmonary delivery of nanoparticle-bound toll-like receptor 9 agonist for the treatment of metastatic lung cancer, ACS Nano 14 (6) (2020) 7200–7215.
[85] X. Chen, L. Zhao, Y. Kang, Z. He, F. Xiong, X. Ling, J. Wu, Significant suppression of non-small-cell lung cancer by hydrophobic poly(ester amide) nanoparticles with high docetaxel loading, Front. Pharmacol. 9 (2018).
[86] J.W. Kytai Nguyen, Serkan Yaman, Harish Ramachandramoorthy, Manoj Kumar Sabnani Double Sided Chimeric Antigen Receptor (CAR) Engineered Cell Membrane Based Drug Delivery System, 2022.
[87] Liu, L.; Pan, D.; Chen, S.; Martikainen, M.-V.; Kårlund, A.; Ke, J.; Pulkkinen, H.; Ruhanen, H.; Roponen, M.; Käkelä, R.; Xu, W.; Wang, J.; Lehto, V.-P., Systematic Design of Cell Membrane Coating to Improve Tumor Targeting of Nanoparticles.
[88] L. Liu, X. Bai, M.-V. Martikainen, A. Kårlund, M. Roponen, W. Xu, G. Hu, E. Tasciotti, V.-P. Lehto, Cell membrane coating integrity affects the internalization mechanism of biomimetic nanoparticles, Nat. Commun. 12 (1) (2021) 5726.